Title (Short title)

Analysis of the influence of peptidoglycan turnover and recycling on host-pathogen interaction in the Gram-positive pathogen *Staphylococcus aureus* (Peptidoglycan recycling and Gram-positive bacteria-host interaction)

Authors

Jack Dorling[1,2] *, Magda Atilano[1,3], Elisabete Pires[4], Errin Johnson[5], Anna Pielach[5,6], James McCullagh[4], Sérgio Filipe[7,8], Petros Ligoxygakis[1] *

Affiliations

[1] New Biochemistry, Department of Biochemistry, University of Oxford, South Parks Road, Oxford, UK

[2] Current address: The John Innes Centre, Norwich Research Park, Norwich, UK

[3] Current address: Institute of Healthy Ageing, Darwin Building, Gower Street, London UK

[4] Chemistry Research Laboratory, Department of Chemistry, University of Oxford, Oxford, UK

[5] Electron microscopy facility, Sir William Dunn School of Pathology, University of Oxford, South Parks Road, Oxford

[6] Current address: Department of Biological and Environmental Sciences, University of Gothenburg, Gothenburg, Sweden

[7] ITQB NOVA, Universidade Nova de Lisboa, Avenida da República, Oeiras, Portugal

[8] Current address: Faculdade de Ciências e Tecnologia, Departamento de Ciências da Vida, Universidade Nova de Lisboa, Caparica, Portugal

* corresponding authors: Jack Dorling (Jack.Dorling@jic.ac.uk) and Petros Ligoxygakis (petros.ligoxygakis@bioch.ox.ac.uk)

Abstract (249 words)

During peptidoglycan recycling (PR) bacteria can recover extracellular fragments of peptidoglycan (PGN) liberated by peptidoglycan turnover (PT) during cell growth and division, and reuse them in cell wall biosynthesis or central carbon metabolism. In Gram-negative bacteria, PR has been well studied, and functions in the induction of resistance to certain classes of antibiotics, and in host-pathogen interaction. However, while Gram-negative cell envelope architecture allows for highly efficient PR, Gram-positive bacteria, which lack an outer cell membrane and are instead enclosed by a glycopolymer layer, can shed large quantities of PGN-derived material to the external environment during growth. Nonetheless, the occurrence of PR was recently demonstrated in several Gram-positive bacteria, including the Gram-positive bacterial pathogen *Staphylococcus aureus*, and its potential adaptive functions are largely unexplored. Given the known roles of PR in Gram-negative bacteria, and that Gram-positive bacteria include several important human pathogens, we asked what role PR may play during Gram-positive pathogen-host interaction. Using

34 the model insect host *Drosophila melanogaster,* we demonstrate that *S. aureus* mutants impaired in
35 extracellular PGN hydrolysis (Δ*atl*) and PGN fragment uptake (Δ*murP*) show differential virulence compared
36 to their wild-type counterpart. This was linked to increased activation of the *D. melanogaster* Toll-cascade by
37 spent supernatant from the Δ*atl* mutant. Thus, we propose that *S. aureus*, and potentially other Gram-
38 positive bacteria, may use extracellular PGN degradation during PT to simultaneously process PGN
39 fragments for recycling and for immune evasion, while recovery and/or metabolism of peptidoglycan
40 fragments during PR may play more subtle roles in determining virulence.
41

42 **Author summary (150 words)**

43 PGN is a key component of the bacterial cell wall, forming a stress-bearing sacculus surrounding the cell and
44 providing cell shape. During growth and division, the sacculus is dynamically degraded and remodelled to
45 ensure daughter cell separation, resulting in PT. PGN fragments released during PT can be recovered and
46 reutilised by the cell during PR. In Gram-negative pathogens, PR is linked to antibiotic resistance, virulence
47 and modulation of host immune recognition. In Gram-positive bacteria, PR was only recently observed. Here,
48 we explore the roles of PT and PR in host-pathogen interaction in *S. aureus, a* Gram-positive pathogen of
49 significant clinical relevance. Disruption of PT in *S. aureus* affected host-pathogen interaction through
50 altering host recognition of shed PGN fragments and PR through modulation of PGN fragment recovery. This
51 improves our understanding of the biology of this important pathogen and may aid development of novel
52 therapeutic approaches to treat *S. aureus* infections.
53

54 **Introduction**

55 Almost all bacteria possess a cell wall (CW) whose main structural component is the PGN sacculus [1]. PGN
56 itself is composed of glycan strands of repeating β-1,4-linked *N*-acetylglucosamine (GlcNAc) and *N*-
57 acetylmuramic acid (MurNAc) disaccharide aminosugar units, cross-linked by short MurNAc-linked peptides
58 [1]. The bacterial PGN sacculus must be sufficiently rigid to resist adverse environmental conditions and
59 rapid changes in osmotic pressure but must also be flexible enough to allow adjustment of CW shape and
60 mechanical properties during growth, division, cell separation and differentiation. As such, the PGN sacculus
61 is constantly remodelled during bacterial growth [2]. Remodelling is carried out by PGN hydrolases
62 (autolysins) produced by bacteria which target covalent bonds within their own PGN sacculi [3].
63

PGN cleavage by autolysins can release CW-derived fragments to the surrounding environment in a process known as CW or PGN turnover. *S. aureus* exhibits CW turnover rates of ~15-25% per generation [4,5] whereas in *Escherichia coli* and *Bacillus subtilis* this is estimated at ~50% [6,7]. PR was first discovered in the Gram-negative *E. coli* [6] where diffusion of CW-derived PGN fragments (muropeptides) is restricted by the bacterium's outer membrane, allowing efficient trapping of most turnover products and their subsequent recovery [6,8]. However, in Gram-positive bacteria such as *B. subtilis* and *S. aureus*, the lack of an outer membrane leads to shedding of large amounts of CW-derived material during growth [9,10]. Indeed, it was previously assumed that Gram-positive bacteria either do not to recycle CW material, or that the process was likely to be of little significance.

Nonetheless, it was recently discovered that Gram-positive bacteria including *S. aureus*, like Gram-negative bacteria, do indeed recycle PGN components of their CW [11,12]. In Gram-negative bacteria, the major PGN recycling substrates are GlcNAc-1,6-anhydro-MurNAc-peptide (GlcNAc-anhMurNAc) fragments [13] produced by cleavage of PGN by lytic transglycosylases which target MurNAc-β-1,4-GlcNAc bonds, generating anhMurNAc-containing muropeptides [3]. These anhydromuropeptides are then taken up via the major facilitator superfamily permease, AmpG [14]. Further catabolism by cytoplasmic PGN hydrolases produces individual aminosugars and amino acids, though larger muropeptide fragments may be directly reused [13]. Individual anhMurNAc residues are then phosphorylated by the kinase AnmK to produce *N*-acetylmuramic acid-6-phosphate (MurNAc-6-P) [15] before processing by MurQ, an etherase that converts MurNAc-6-P to GlcNAc-6-P [16].

In *E. coli*, individual MurNAc residues may also be recovered via MurP, a phosphotransferase system (PTS) component, which phosphorylates MurNAc during uptake, producing MurNAc-6-P [17]. While orthologues of AmpG are generally missing in Gram-positive bacteria, including *S. aureus*, orthologues of both MurP and MurQ are found in these bacteria [9]. Indeed, *S. aureus* can take up MurNAc from the growth medium via MurP and convert the resulting MurNAc-6-P to GlcNAc-6-P via MurQ [11]. In *S. aureus*, as in *E. coli*, recycling then proceeds via the enzyme NagA, which can deacetylate GlcNAc-6-P to produce glucosamine-6-P (GlcN-6-P) [18,19] which may then enter glycolysis after conversion to Fructose-6-phosphate (Fru-6-P), or be reused directly for PGN biosynthesis. However, unlike *E. coli*, in which recycling continues throughout growth, recycling in *S. aureus* becomes detectable only after the transition of the bacterial culture from exponential growth phase to stationary phase has begun [11,12].

96 *S. aureus* also extensively *O*-acetylates MurNAc residues within the PGN sacculus, rendering it extremely
97 resistant to host-produced lysozyme-like *N*-acetylmuramidases [20]. Aside from two putative lytic
98 transglycosylases with unknown cleavage specificity, *S. aureus* also does not appear to encode such
99 enzymes in its genome [21]. The combined activity of peptidoglycan hydrolases of *S. aureus* is thus
100 expected to produce MurNAc-β-1,4-GlcNAc (MurNAc-GlcNAc) PGN fragments (**Fig. 1a**), which likely
101 represents the major PR substrate of *S. aureus*, and is taken-up via MurP in this organism [12] (**Fig. 1a**).
102 Following uptake and concomitant phosphorylation of MurNAc-GlcNAc by MurP, MurNAc-6-P-GlcNAc is then
103 cleaved by the cytoplasmic PGN hydrolase MupG to form MurNAc-6-P and GlcNAc [12] (**Fig. 1a**). MurNAc-
104 6-P is then processed by MurQ as in *E. coli*. The fate of the unphosphorylated GlcNAc residue (**Fig. 1a**) is
105 currently unknown [12]. The genes *mupG, murQ* and *murP* are encoded together in a PR operon, along with
106 *murR*, which encodes an RpiR/AlsR family transcriptional regulator [11,22] (**Fig. 1b**).
107
108 Although it has now been established that PR occurs in *S. aureus* and other Gram-positive bacteria, the
109 likely adaptive function of this process in this group is still unclear. In *B. licheniformis*, uptake of PGN-derived
110 peptides has been implicated in the modulation of antibiotic resistance [23] while in *M. tuberculosis* antibiotic
111 resistance induction was linked to aminosugar recycling [24]. Similarly, *S. aureus nagA* mutants are also
112 affected in their resistance to antibiotics [19]. *S. aureus* lacking *murQ also* suffers a minor survival
113 disadvantage during prolonged stationary phase in LB medium [11]. However, while Gram-negative PR plays
114 roles in regulating β-lactamase expression in a number of Gram-negative species [25], it also plays roles in
115 virulence regulation in *Salmonella enterica* serovar *Typhimurium [26]* and in regulation of host-pathogen
116 interaction in *Neisseria* spp. and *Shigella flexneri* [27,28]. Indeed, in *M. tuberculosis,* PGN aminosugar
117 recycling was also linked to lysozyme resistance *in vitro* [24].
118
119 Given that sugar uptake plays a major role in the pathogenic lifestyle of *S. aureus* [29] we hypothesised that
120 PR might also play roles in host-pathogen interaction during *S. aureus* infection. To test this, we generated
121 and characterised a panel of markerless *S. aureus* deletion mutants lacking genes encoding key
122 components of the PR pathway in this organism, namely *murP, murQ* and *nagA* (**Fig 1a**, **b**; PR mutants),
123 which are impaired in their ability to take up and reutilise MurNAc-containing PGN fragments, and challenged
124 the model host *D. melanogaster* with these strains. We discovered that *S. aureus* Δ*murP,* which is unable to
125 recover MurNAc-containing PGN fragments from the medium was compromised in its virulence in this model
126 system, while the other two mutants, which can recover such PGN fragments but are impaired in their ability
127 to reutilise this material, behaved as the wild-type strain.

128

129 The three mutants produced PGN and a bacterial cell surface of similar composition, and we established that
130 the difference in their ability to kill flies or survive the innate immune system was not linked to their modified
131 immune recognition, nor to modified lysozyme resistance as shown for other *S. aureus* mutants impaired in
132 PGN metabolism [30]. Instead, we hypothesise that this is potentially linked to impacts on virulence
133 regulation. In the process of conducting these experiments, we also discovered that spent culture
134 supernatant (SCS) of *S. aureus* lacking Atl (Δ*atl*), the major autolysin of *S. aureus* (**Fig. 1a**) strongly
135 stimulated the *D. melanogaster* immune response. This suggests that the degree of cleavage of released
136 PGN fragments and the quantity of fragments present in the medium, which may also influence or be
137 influenced by PR, is important in immune evasion by this organism.

138

139 Results

140 Growth parameters of PR mutants

141 We grew the 'wild-type' parental strain of *S. aureus* NCTC8325-4 (NCTC) and derived PR mutants in rich
142 media (TSB; tryptic soy broth) to determine their growth parameters. All of the PR mutants generated in this
143 study (**S1 Table**) showed no differences in their growth rates in rich media (**Fig. 2**, **S2 Table**; Analysis of
144 variance (ANOVA); $F_{3, 8}^{bacterial_strain} = 3.01$, $p = 0.095$). However, Δ*murP* and Δ*nagA* were unable to reach the
145 same maximum OD_{600} as NCTC or Δ*murQ* (**Fig. 2**, **S2 Table**; ANOVA; $F_{3, 8}^{bacterial_strain} = 12.4$, $p < 0.01$). Δ*murQ*
146 also lost a smaller percentage of maximum OD_{600} after growth halted (**Fig. 2**, **S2 Table**; ANOVA; $F_{3, 8}$
147 $^{bacterial_strain} = 14.5$, $p < 0.01$). These data, in accordance with a previous report [11], demonstrate the lack of an
148 observable impact of removal of PR enzymes during exponential growth in rich media where the bacteria are
149 not exposed to any particular environmental stresses.

150

151 Dynamics of GlcNAc-6-P accumulation in NCTC and Δ*nagA*

152 As it has already been established that PR is most active during transition and stationary phase in *S. aureus*,
153 and that MurNAc-6-P and MurNAc-6-P-GlcNAc accumulate in the cytoplasm during this period in mutants
154 lacking *murQ* and *mupG*, respectively [11,12], we decided to establish whether this was also the case for
155 GlcNAc-6-P in our Δ*nagA* mutant. In this mutant, which has a functional MurP transporter and a functional
156 MurQ etherase capable of converting MurNAc-6-P to GlcNAc-6-P, the uptake of GlcNAc by (an)other PTS
157 transporter(s) [28, J. Dorling unpublished data] may influence the impact of recycling of different

158 aminosugars on *S. aureus* physiology or host-pathogen interaction. Indeed, we had already observed that
159 Δ*nagA* reached a lower maximum OD_{600} than NCTC (**Fig. 2**).
160
161 Metabolite analysis of cytoplasmic content extracted from NCTC and Δ*nagA* grown in TSB, revealed that
162 Δ*nagA* accumulated significantly more GlcNAc-6-P than NCTC (**Fig. 3**; Analysis of Deviance (ANODE); χ^2
163 $^{time_point\ :\ bacterial_strain}$ = 6.97, df = 2, $p < 0.001$) and that this was indeed higher during transition phase (2.46 ±
164 0.62-fold) and stationary phase (1.51 ± 0.43-fold) than during exponential phase. Interestingly, cytoplasmic
165 GlcNAc-6-P abundance in NCTC fell during this period (**Fig. 3**, transition; 4.81 ± 2.4-fold, stationary; 7.41 ±
166 7.2-fold) and in Δ*nagA* appeared to peak during transition phase (**Fig. 3**).
167
168 **Impact of *nagA* deletion on downstream metabolite accumulation**
169 NagA is the link between PR-specific metabolic activities and central carbon metabolism / PGN
170 (re)biosynthesis [19] (**Fig. 1**). Thus, we sought to determine if the abundances of metabolites downstream of
171 NagA were affected, to help understand whether blocking of the reutilisation of material recovered by PR
172 may have knock-on effects on *S. aureus* metabolism, under the investigated conditions.
173
174 To do so, we examined the abundances of GlcN-6-P, the product of NagA deacetylation of GlcNAc-6-P and
175 the hub between PR and CW biosynthesis, and Fru-6-P, the hub between PGN metabolism and glycolysis
176 [19] (**S1 Fig**). This revealed that while no differences in the abundance of GlcN-6-P were detectable between
177 NCTC and Δ*nagA* (**S1a Fig**; ANOVA; $F_{2,\ 26}{}^{bacterial_strain}$ = 0.011, p = 0.92). Fru-6-P abundances peaked in
178 transition phase in both NCTC and Δ*nagA*, dropping in stationary phase, while still remaining at levels higher
179 than during exponential phase (**S1b Fig**). However, the peak abundance of Fru-6-P in transition phase was
180 lower (1.24 ± 0.21-fold) in Δ*nagA* than in NCTC (**S1b Fig**; ANOVA; $F_{2,\ 24}{}^{time_point\ :\ bacterial_strain}$ = 3.99, $p < 0.05$).
181
182 **Stationary-phase viability of PR mutants**
183 Having now established that the dynamics of GlcNAc recycling via NagA were similar to those of MurNAc
184 recycling, and that deletion of *nagA* led to slightly smaller pools of GlcN-6-P available for PGN biosynthesis,
185 we then wanted to establish whether a similar minor survival disadvantage during stationary phase as that
186 previously observed in an *S. aureus* Δ*murQ* mutant could also be observed in Δ*nagA* [11]. Thus, we tested
187 the ability of our PR mutants to maintain viability during stationary phase in rich TSB medium (**Fig. 4**). While
188 a slight reduction in viability of Δ*murQ* relative to other PR mutants was observed at 24h and 72h post-
189 inoculation (ANODE; $\chi^{2\ time_point\ :\ bacterial_strain}$ = 4.26×10^9, df = 12, $p < 0.05$), we did not document a significant

190 reduction in Δ*murQ* viability relative to wild-type *S. aureus* (NCTC) as previously observed in LB medium
191 [11], nor did we observe any differences in viability of the other PR mutants relative to NCTC (**Fig. 4**).
192
193 **Virulence and *in vivo* bacterial load of PR mutants in *D. melanogaster***
194 After establishing the apparent lack of a survival disadvantage under nutrient limitation for any of our PR
195 mutants, we wanted to address our main hypothesis; that PR may play a role in governing host-pathogen
196 interaction in *S. aureus.* To do so, we infected *D. melanogaster* isogenic line *25174,* a line established by the
197 *Drosophila* genetics reference panel (DGRP) [31]. We examined host survival as a proxy for bacterial
198 virulence, as well as *in vivo* bacterial load to distinguish between the overall bacterial load within the host and
199 their intrinsic virulence. As Atl also plays an important role in *S. aureus* PR [12], and as *S. aureus* Δ*atl*
200 mutants are known to show reduced virulence in this model host [32], we included an *S. aureus* Δ*atl* mutant
201 in these experiments.
202
203 These experiments revealed that while neither Δ*murQ* nor Δ*nagA* showed differential virulence when
204 compared to NCTC, Δ*murP* was less capable of killing *D. melanogaster* over the assayed 72h period (**Fig.**
205 **5a**; log-rank test; $\chi^{2\ \text{bacterial_strain}} = 442$, df = 5, $p < 0.001$). However, despite showing reduced virulence relative
206 to NCTC, the impairment of virulence was far less than that of Δ*atl* (**Fig. 5a**), which showed comparable
207 patterns of killing to those previously observed [32]. Indeed, while considerably reduced *in vivo* bacterial
208 loads of Δ*atl* were also observed relative to NCTC (**Fig. 5b**; ANOVA; $F_{4,\ 81}{}^{\text{bacterial_strain}} = 14.2$, $p < 0.001$), Δ*murP*
209 had a comparable bacterial load to NCTC within the host (**Fig. 5b**).
210
211 **Immune stimulation by spent PR mutant culture supernatants**
212 Having already collected data suggesting only very subtle differences in the CW structure between PR
213 mutants (**S2 Fig**), we reasoned that this was unlikely to explain the differences in Δ*murP* virulence we
214 observed in **Fig. 5a**. However, as Δ*murP* mutants of *S. aureus* accumulate MurNAc-GlcNAc disaccharides
215 extracellularly [12], which should not occur in either of the other PR mutants tested, we considered a different
216 hypothesis. We asked whether the increased extracellular accumulation of MurNAc-GlcNAc disaccharides
217 may potentially activate the *D. melanogaster* Toll-cascade via PGRP-SA and contribute to the reduced
218 virulence of Δ*murP.* Multiple *S. aureus* PGN-derived molecules have been tested for their
219 immunostimulatory activity in *D. melanogaster* [33], but no data exists for the immunostimulatory activity of
220 this molecule, nor when present together with the infecting microorganism.

221

222 To test this hypothesis, we grew cells to stationary phase and isolated 0.22µm-filtered SCS. We then injected
223 this into *D. melanogaster* flies containing a Drosomycin-GFP fusion (*DD1* flies), as well as their counterparts
224 lacking PGRP-SA and the ability to detect Gram-positive PGN (*DD1*^{seml} flies). We quantified GFP
225 fluorescence in injected flies 18h post-injection (**Fig. 6**). We included Δ*atl* SCS in these experiments as a
226 mutant expected to elicit differential immunostimulatory activity to NCTC due to reduced PGN-trimming from
227 the cell surface of this strain [32]. In addition, any PGN fragments released from this strain may not be
228 processed as in the parental strain as other hydrolases are present in the supernatant in differing quantities
229 in Δ*atl* SCS [34]. We have also previously observed that polymerised muropeptides elicit a stronger
230 immunostimulatory activity than monomeric muropeptides [33].

231

232 We found that SCS of Δ*murQ* and Δ*murP* elicited a very modestly reduced immunostimulatory capacity in
233 both *DD1* flies and *DD1*^{seml} flies (**Fig. 6**; ANODE; $\chi^{2\ \text{bacterial_strain : fly_line}} = 47.8$, df = 4, $p < 0.001$). However, while
234 statistically significant, differences of such small magnitude are unlikely to be of biological significance.
235 Unexpectedly however, we found that Δ*atl* SCS possessed a much higher immunostimulatory capacity than
236 SCS from NCTC or the PR mutants, though only in *DD1* flies (**Fig. 6**), suggesting that this is effect is most
237 likely linked to PGN-derived material in the SCS of Δ*atl*.

238

239 **Virulence and *in vivo* bacterial load of PR mutants in PGRP-SA-deficient *D. melanogaster* hosts**

240 As we had not observed any differences increased immunostimulation by Δ*murP* SCS, we decided to check
241 whether the same reduced efficiency of the killing of *D. melanogaster* by this mutant was observed in the
242 absence of functional PGRP-SA (**Fig. 7a**). Indeed, when we infected *D. melanogaster 25714*^{seml} flies, which
243 lack a functional copy of PGRP-SA and generally die more rapidly upon infection, we observed the same
244 reduced virulence of Δ*murP* relative to NCTC and the other PR mutants (**Fig. 7a**; log-rank test; $\chi^{2\ \text{bacterial_strain}} =$
245 629, df = 5, $p < 0.001$). However, in this fly genetic background Δ*atl* showed comparable virulence to NCTC
246 (**Fig. 7a**), as previously observed [32]. This confirmed that the differential virulence of Δ*murP* was not linked
247 to PGRP-SA mediated recognition of PGN in this mutant. We also observed no differences in the bacterial
248 load between any of the mutants in *25714*^{seml} flies (**Fig 7b**; ANOVA; $F_{4,\ 38}{}^{\text{bacterial_strain}} = 1.57$, $p = 0.20$).

249

250 **Lysozyme resistance of PR mutants**

251 As differential virulence was not based on differential recognition of Δ*murP*, this difference in virulence had to
252 be otherwise explained. Despite the intrinsic lysozyme resistance of *S. aureus* thanks to extensive *O*-

253 acetylation of its PGN [20], a similar virulence phenotype, in which an *S. aureus* strain expressing a minimal
254 PGN biosynthesis machine showed decreased virulence in both *25174* and *25174*^{seml} flies, was previously
255 explained by a decrease in lysozyme resistance in this strain [30]. Additionally, PR has also been shown to
256 be involved in modulating lysozyme resistance via an unknown mechanism in *M. tuberculosis* [24]. We
257 therefore reasoned that perhaps perturbation of PR might also affect lysozyme resistance. Thus, we
258 subjected our PR mutants to a lysozyme-resistance assay (**Fig. 8**), including a Δ*tagO* mutant as a positive
259 control known to be more sensitive to lysozyme (**S1 Table**). However, we found no difference in the
260 lysozyme resistance of the PR mutants relative to NCTC, and instead found only an impact of *tagO* deletion
261 (**Fig. 8**; ANOVA; $F_{4, 190}^{\text{time_point : lysozyme_treatment : bacterial_strain}} = 8.70$, $p < 0.001$).
262

263 ## Discussion

264 To date, only a handful of studies have addressed the topic of PR in Gram-positive bacteria [11,12,35–39]
265 and only in recent years has PR been shown to occur in this group [11,12,24,38,40]. However, the
266 physiological function of this process in Gram-positive bacteria remains largely unexplored with only some
267 indication that Gram-positive PR may play a role in the maintenance of bacterial viability under nutrient
268 limiting conditions [11,12,35] and that PR may play an important role in antibiotic and lysozyme resistance
269 [19,23,24].
270

271 Here, while documenting some differences in growth characteristics of our PR mutants we were unable to
272 confirm a previously detected survival defect of Δ*murQ* under nutrient-limitation [11], nor to detect such a
273 disadvantage in our Δ*murP* or Δ*nagA* mutants. However, while both our study and that of Borisova *et al*.
274 used rich media, we employed TSB while they used LB medium. We did however show that GlcNAc-6-P
275 accumulated in the cytoplasm of Δ*nagA* in a similar manner to MurNAc-6-P in an *S. aureus* Δ*murQ* mutant,
276 confirming that PR is indeed most active during stationary phase and transition phase in this organism.
277 However, we also documented that this had very little or no impact on the downstream abundance of GlcN-6-
278 P or Fru-6-P, and likely has little impact on PGN biosynthesis and central carbon metabolism under these
279 conditions.
280

281 Δ*nagA* did however display a very modest reduction in Fru-6-P abundance during transition phase. GlcNAc-
282 6-P abundance also fell in the cytoplasm of NCTC during this period. As Fru-6-P is the hub metabolite
283 between PR and glycolysis, this suggests that PR may provide some energy for a final round of cell division

284 during the entry into stationary phase, as suggested from studies of Gram-negative bacteria [13]. Taken
285 together, these results suggest that while PR may function in supplying energy to the cell under nutrient
286 limitation, its function in maintaining bacterial viability [11] is likely a minor one. However, experiments in
287 more realistic physiological conditions, or over longer timescales, would be required to confirm this.
288
289 Here, we report that *S. aureus* mutants impaired in their ability to recover MurNAc-GlcNAc disaccharides
290 during PR (Δ*murP*) and in the generation of these disaccharides during PGN turnover (Δ*atl*) are both less
291 virulent than their wild-type counterparts. While the impaired virulence of Δ*atl* was already documented, we
292 extend the characterisation of this phenotype, demonstrating that the absence of functional Atl not only
293 increases PGRP binding to the cell surface [32], but that spent culture supernatant of Δ*atl* bacteria also
294 elicits a robust PGRP-mediated immune response in our model host. As this was only observed in *DD1* flies
295 possessing a functional PGRP-SA, this suggested that a decreased or aberrant hydrolysis of shed PGN-
296 derived material was responsible for this result. While we also documented differences in the
297 immunostimulatory capacity of SCS of Δ*murQ* and Δ*murP* these differences were small in magnitude and
298 likely of little biological significance. We therefore could not correlate this result with the observed patterns of
299 virulence or *in vivo* bacterial loads.
300
301 While the process of PR itself begins with the uptake of liberated PGN fragments by the cell which produced
302 them, PGN fragments must first be generated by the action of PGN hydrolases [9]. Due to the high degree of
303 *O*-acetylation of MurNAc residues in the PGN of *S. aureus*, this bacterium likely uses mainly, or exclusively,
304 *N*-acetylglucosaminidases alongside amidases and endopeptidases to degrade its PGN during cell growth.
305 *S. aureus* possesses multiple *N*-acetylglucosaminidases including Atl, the major autolysin, as well as SagA,
306 SagB, and ScaH [41–43], which function alongside amidases and endopeptidases to generate MurNAc-
307 GlcNAc fragments, the major PR substrate of *S. aureus* [12].
308
309 SagA, SagB, and ScaH are *N*-acetylglucosaminidases required for proper septum formation during the final
310 stage of cell division. SagB also shortens of newly synthesized glycan strands to ensure flexibility during cell
311 elongation [41]. Atl on the other hand is a multi-domain protein, containing *N*-terminal *N*-acetylmuramoyl-L-
312 alanine amidase and C-terminal endo-β-*N*-acetylglucosaminidase domains [42]. Proteolytic cleavage of the
313 Atl propeptide generates two different PGN hydrolases, which have functions in cell expansion and division,
314 and are required for proper daughter cell separation [42,44].
315

316 Atl is already known to trim excess PGN from the bacterial cell surface, reducing PGRP binding [32]. Atl is
317 also secreted into the external environment by *S. aureus* [42] and the two PGN hydrolases encoded by *atl*
318 alone can generate MurNAc-GlcNac fragments. The discovery here that SCS from Atl mutants elicits a
319 PGRP-SA dependent immune response in *D. melanogaster* highlights that Atl, and potentially other
320 autolysins [34], also play an important role in decreasing immune stimulation by shed PGN fragments while
321 simultaneously generating fragments that can be recycled by *S. aureus*.
322
323 PGN shedding is characteristic of many [45], but not all [39,45,46], Gram-positive bacteria, and external PGN
324 hydrolysis is also a known feature of PR in other Gram-positives [35]. For pathogenic Gram-positive-bacteria
325 bacteria like *S.* aureus, this may aid in avoiding immune recognition by the host, given the large quantities of
326 PGN-derived material shed by this organism. Similarly, generation of MurNAc-GlcNAc fragments may allow
327 cell-cell communication [47], perhaps via MurP mediated uptake of fragments originating from neighbouring
328 *S. aureus* bacteria.
329
330 MurNAc-GlcNac fragments generated by the action of Atl and other PGN hydrolases are taken-up via MurP
331 [12] before metabolism in the *S. aureus* cytoplasm. We also documented that Δ*murP* displayed reduced
332 virulence when compared to its wild-type counterpart. However, unlike the reduced virulence of Δ*atl*, this
333 phenotype could not be linked to increased recognition of accumulated of MurNAc-GlcNAc in the
334 supernatant of this mutant [12]. Indeed, we also demonstrated that Δ*murP* displayed reduced virulence in *D.*
335 *melanogaster* lacking functional PGRP-SA. It may also be possible that the increased quantities of PGN-
336 derived fragments in the medium may activate the *D. melanogaster* immune system in a PGRP-SA
337 independent manner, but if so this did not translate into reduced bacterial load (**Fig. 5b**, **Fig 7b**). We also
338 established that this reduced virulence was not explained by altered lysozyme susceptibility in this mutant, as
339 had been seen for an *S. aureus* mutant possessing minimal PGN biosynthesis machinery [30].
340
341 To try and better understand this phenotype, we turned out attention to the other genes present in the same
342 operon as *murP* (**Fig. 1a**). One of these genes, encoding MupG, has recently been characterised and was
343 shown to encode a cytoplasmic PGN hydrolase responsible for the cleavage of MurNAc-6-P-GlcNAc to
344 produce MurNAc-6-P and GlcNAc [12]. The other encodes MurR [11,12] which has also been partly
345 characterised [22]. MurR, encoded by *murR*, is also known as RpiRB and is involved in regulating pentose
346 phosphate pathway activity and virulence factor production in *S. aureus* as a response to TCA cycle stress

347 resulting from nutrient limitation [22]. Deletion of *murR* also results in increased production of RNAIII and a
348 decreased rate of haemolysis [22], and therefore likely plays a role in regulation of virulence in *S. aureus*.
349
350 MurR belongs to the RpiR/AlsR family of transcriptional regulators, whose members contain highly
351 conserved DNA-binding N-terminal helix-turn-helix domains and C-terminal sugar phosphate
352 isomerase/sugar phosphate binding domains. The orthologue of MurR in *E. coli* [11] regulates expression of
353 MurNAc utilisation genes in a MurNAc-6-P-dependent manner [48]. A similar interaction with MurNAc-6-P in
354 *S. aureus* may also occur, though this is unknown. MurNAc-6-P accumulation is greatest under nutrient
355 limitation (i.e. in stationary phase) and MurNAc-6-P may act as a signal to trigger virulence factor production
356 via MurR. As cytoplasmic MurNAc-6-P accumulation in *murP* mutants does not occur [11,12], this could
357 explain why the virulence of this strain is impaired. Indeed, it is becoming increasingly recognised that
358 perturbations in metabolism alter virulence factor production and infection outcomes in *S. aureus* [49].
359
360 Accumulation of PR intermediates in the Gram-negative *Salmonella enterica* also alters virulence of this
361 pathogen [26] and PGN metabolites are important regulatory signals involved in multiple other cellular
362 processes in Gram-positive bacteria, including antibiotic resistance [23,47]. Alternatively, extracellularly
363 accumulated MurNAc-GlcNAc fragments in Δ*murP* mutants [12], may bind the extracellular penicillin binding-
364 associated and serine/threonine kinase-associated (PASTA) domain of the *S. aureus* serine-theonine kinase
365 Stk1 [50], which is also involved in virulence regulation in this bacterium [51].
366
367 In conclusion, *S. aureus* appears to employ extracellular PGN hydrolysis to degrade fragments of PGN
368 released as a result of cell growth and division processes to avoid activation of host immune responses,
369 while simultaneously preparing this material for recovery by the cell. Uptake of this maximally-hydrolysed
370 PGN-derived material [12] may then be used to support *S. aureus* metabolism to some extent, but may also
371 influence expression of virulence, potentially via MurR-mediated virulence regulation. Ultimately, PR appears
372 to be important in *S. aureus* host-pathogen interaction, and further investigation into the role of PR in Gram-
373 positive bacterial virulence would be of great interest, particularly in a mammalian model host.
374

375 ## Materials and Methods

376 **Bacterial strain construction**

377 *S. aureus* NCTC8325-4 (NCTC) was used as the main 'wild-type' strain. The construction of Δ*murP*, Δ*murQ*
378 and Δ*nagA* PR mutant strains was performed as initially described by Arnaud *et al.* [52], using the plasmids
379 listed in **S1 Table**
380
381 To construct these mutants, we amplified ~800-900bp regions upstream (**S4 Table**; 'p1' and 'p2' primers for
382 each respective gene) and downstream (**S4 Table**; 'p3' and 'p4' primers for each respective gene) of each
383 respective gene. The resulting PCR products were joined by overlap PCR using 'p1' and 'p4' primers for
384 each gene. This product was then digested with the respective restriction endonuclease enzymes (New
385 England Biolabs) listed in **S4 Table**, allowing their subsequent ligation into a similarly digested pMAD [52]
386 vector backbone. The constructed plasmids are listed in **S1 Table**. The plasmids were sequenced using the
387 primers listed in **S4 Table**, and introduced into RN4220 (**S1 Table**) by electroporation. Following
388 electroporation, plasmids were transduced using phage 80α to NCTC as previously described [53]. Insertion
389 and excision of plasmids into the NCTC chromosome was performed as previously described [52]. Features
390 of bacterial strains are listed in **S1 Table**.
391
392 PCR confirmation of mutant genotypes, as well as absence of the pMAD vector used for deletion, is given in
393 **S4 Fig**. Enzymes for DNA restriction and cloning, as well as 1kB DNA ladder were purchased from New
394 England Biolabs while GoTaq PCR reagents (Promega) were purchased from Thermo Fisher Scientific.
395 QIAquick PCR cleanup and QIAprep Spin Miniprep kits were obtained from Qiagen. Primers were designed
396 using Primer3plus (www.bioinformatics.nl/cgi-bin/primer3plus/primer3plus.cgi/), ReverseComplement
397 (www.bio-informatics.org/sms/rev_comp.html) and OligoCalc (http://biotools.nubic.northwestern.edu/
398 OligoCalc.html) and resulting oligonucleotides purchased from Life Technologies (Thermo Fisher Scientific).
399 Both plasmids and final deletion mutants were sequenced by Sanger sequencing to confirm the sequence of
400 the deleted region. Primer sequences can be found in **S4 Table**.
401
402 **DNA purification**
403 DNA was extracted from *S. aureus* for deletion fragment amplification and confirmation of mutant identity.
404 Cells were resuspended in EDTA (50mM, pH 8.0) containing Lysostaphin and RNase A before shaking at
405 37°C for 30min. Further EDTA and nuclei lysis solution (Promega) were added. The mixture was incubated at
406 80°C for 10min and cooled to RT. Protein precipitation solution (Promega) was added and samples were
407 vigorously mixed. Samples were incubated for 10min on ice, debris pelleted and supernatant was transferred
408 to a fresh tube. Propan-2-ol was added mixed by inversion. Samples were centrifuged, supernatant carefully

409 removed and samples air-dried. 70% (v/v) ethanol was added and tubes were inverted several times.
410 Samples were centrifuged again, ethanol carefully removed and samples air-dried. DNA was dissolved in
411 distilled water. Plasmids transformed into DH5α competent cells were purified from overnight cultures using a
412 QIAprep Spin Miniprep Kit. DNA concentrations were measured using a Nanodrop1000 (Thermo-Fisher
413 Scientific).
414
415 **Bacterial growth conditions**
416 *S. aureus* strains were routinely grown in TSB (Difco) at 180rpm, or on tryptic soy agar (TSA; TSB with 1.5%
417 added agar, Difco). Bacteria were grown at 30°C to enable comparison of results between *in vitro* and *in vivo*
418 infection experiments (see *D. melanogaster* rearing below). Overnight cultures (~16h) were used to inoculate
419 fresh medium at an initial optical density at 600nm (OD_{600}) of 0.05. A ratio between the volumes of liquid and
420 air of 1:5 was maintained for adequate aeration of cultures. Bacteria were plated from -80°C glycerol stocks
421 on TSA at most 3 days before use in experiments.
422
423 **Analysis of bacterial growth parameters and viable cell counts**
424 To analyse bacterial growth OD_{600} of bacterial cultures was measured using an Amersham Pharmacia
425 Biochrom Ultrospec 2100 spectrophotometer. For growth experiments in TSB, r_0 values were calculated
426 using the `R` package `grofit` [54]. Maximum and final OD_{600} measures were extracted from the data using
427 appropriate functions in `R` and percentage OD_{600} loss calculated as the difference between the two values
428 divided by maximum OD_{600}. For experiments examining cell viability samples were taken, placed on ice,
429 serially diluted in fresh ice-cold TSB and 100µL of pre-determined dilutions plated with glass beads on TSA
430 plates to achieve colony counts of ~30-300 colonies. Plates were incubated for ~30h at 30°C and
431 photographed. Colonies were enumerated using the automatic colony counting program OpenCFU [55].
432
433 **Extraction of cytoplasmic content for metabolite analysis**
434 Bacteria from overnight cultures were inoculated at an initial OD_{600} of 0.05 in triplicate Erlenmeyer flasks
435 containing 200mL fresh TSB. One of each triplicate was collected at 6h, 12h and 24h of growth, OD_{600}
436 measurements taken, and flasks chilled in an ice-ethanol bath for 10 minutes. Entire cultures were pelleted
437 at 5000 x *g* for 15 minutes at 4°C, supernatants entirely removed by aspiration and pellets snap frozen in
438 liquid nitrogen. Samples were stored at -80°C before further processing.
439

440 Frozen cell pellets were defrosted on ice and re-suspended to a final OD_{600} of 250. 1mL of sample was
441 homogenised with 250mg of fine (0.25 - 0.5mm) acid-washed glass beads in a FastPrep-24 Classic (MP
442 Biomedicals). 4 x 35s cycles of homogenisation at 6.5m s^{-1} were used, incubating samples on ice for 2
443 minutes after the first two cycles. Homogenised samples were pelleted at 16,000 x *g* for 10 mins at 4°C.
444 500µL of supernatant was then filtered through pre-washed 0.5mL 3kDa molecular weight cut-off filters
445 (Amicon) by centrifugation at 14,000 x *g* for 20 minutes at 4°C. Filtered supernatants were then lyophilised at
446 55°C in a CentriVap Benchtop Centrifugal Vacuum Concentrator (Labconco) until complete dryness (~4h).
447 Samples were then stored at -20°C.
448
449 **Metabolite profiling by IC-MS/MS and specific identification of GlcNAc-6-P**
450 Cytoplasmic extracts were placed on ice and dissolved in 80% (v/v) LC/MS grade methanol:water. Analysis
451 of cytoplasmic metabolite content was performed at the Mass Spectrometry Research Facility (Department
452 of Chemistry, University of Oxford) using a Thermo Fisher Scientific ICS-5000+ ion chromatography system
453 coupled directly to a Q-Exactive HF Hybrid Quadrupole-Orbitrap mass spectrometer with a HESI II
454 electrospray ionisation source (Thermo Fisher Scientific), using a modified version of the previously
455 published method [56].
456
457 A 10µL partial loop injection was used for all analyses and the chromatographic separation was performed
458 using a Thermo Fisher Scientific Dionex IonPac AS11-HC 2x250mm ion chromatography (IC) column, (4µm
459 particle size) with an in-line Dionex Ionpac AG11-HC 4µm 2x50mm guard column. This system incorporates
460 an electrolytic anion generator (KOH) which produces an OH^- gradient from 5-100mM over 37min at a flow
461 rate of 0.250mL min^{-1} for analyte separation. An in-line electrolytic suppressor was employed to remove OH^-
462 ions and cations from the post-column eluent prior to delivery to the MS system electrospray ion source
463 (Thermo Fisher Scientific Dionex AERS 500).
464
465 Analysis was performed in negative ion mode using a scan range of 80-900 and the resolution set to 70,000.
466 The tune file source parameters were set as follows: sheath gas flow; 60 ms^{-1}, auxiliary gas flow; 20ms^{-1},
467 spray voltage; 3.6 V, capillary temperature; 320°C, S-lens retardation factor value; 70, heater temperature;
468 450°C. The automatic gain control target was set to $1x10^6$ and the maximum ionisation time value was
469 250ms. The column temperature was kept at 30°C throughout the experiment and full scan data were
470 acquired in continuum mode across a mass-to-charge ratio (m/z) range of 60-900. The m/z of a GlcNAc-6-P
471 standard (Sigma-Aldrich) was determined as 300.049 with a column retention time of 12.41 minutes (data

472 not shown). This information was used to identify the peak of interest. Both GlcN-6-P (m/z; 258.038,
473 retention time; 13.15 minutes) and Fru-6-P (m/z; 259.022, retention time; 14.09 minutes) were compounds
474 already present in the compound library of the Mass Spectrometry facility at the Chemical Research
475 Laboratory, University of Oxford. Data were acquired and analysed using Xcalibur and Progenesis software
476 (Thermo Fisher Scientific).
477
478 ***D. melanogaster* lines, rearing and injection**
479 *D. melanogaster* flies were raised at 25°C with a 12h:12h light:dark cycle. Flies were fed on food containing
480 7.69g L^{-1} agar, 34.6g L^{-1} maize, 4.15g L^{-1} soya, 7.04g L^{-1} yeast, 69.2g L^{-1} malt, and 19.2 mL L^{-1} molasses.
481 Flies were routinely cultured in bottles containing ~50mL food, but prior to infection were housed in groups of
482 15-20 flies in observation vials containing ~10mL food. Fly lines used in this study are listed in **Table 1**. Flies
483 were used 3-5 days post-eclosion as adults. Flies were shifted to 30°C 24h before infection and kept at this
484 temperature for the duration of infection experiments. A temperature of 30°C was chosen as the survival of *D.*
485 *melanogaster* is affected at 37°C, while a normal rearing temperature of 25°C for *D. melanogaster* prevents
486 rapid bacterial growth during infection. Incubation at 30°C permits meaningful infection experiments to be
487 carried out. This determined bacterial growth temperature for other experiments.
488
489 Overnight bacterial cultures of 20mL were pelleted at 5000 x *g* for 10 minutes at 4°C, washed twice with PBS
490 (137mM NaCl, 2.7mM KCl, 10mM Na_2HPO_4, 1.8mM KH_2PO_4, pH 7.4) and finally re-suspended in PBS and
491 diluted to pre-determined concentrations to ensure injection of ~100-200 CFU per fly per injection. Inoculates
492 were prepared on ice. In the case of injection of spent bacterial culture supernatants, supernatants were
493 saved from 20mL overnight cultures, filtered through 0.2µm filters, adjusted to an equivalent concentration of
494 OD_{600} 5.0 and stored on ice before injection into Drosophila. Bacterial cells and spent culture supernatant
495 samples were injected into Drosophila via the anepisternum (a soft area of the thorax, below the wing) of
496 adult flies using a Nanoject II microinjector (Drummond Scientific) via pulled glass capillary needles.
497
498 ***D. melanogaster* survival, *in vivo* bacterial titres and immune stimulation by spent culture medium**
499 After infection, survival of *25174* and *25174*^{seml} flies was assayed at 0h, 3h, 6h, 12h and then every 4-12h for
500 72h. Those flies dying within the first 6h of infection were excluded from analysis as they represent
501 casualties caused by injection. The number of flies excluded was usually between 0-2 and did not exceed 4
502 on any occasion. Survival data from experiments monitoring *in vivo* bacterial titres were combined with
503 experiments used purely for assessment of survival, with censoring of flies sampled for bacterial titre

504 determination as appropriate. In *25174*^{seml} replicates 5 and 6, surviving PBS injected flies were censored at
505 36h as all other flies were used for CFU sampling or were dead. Bacterial infection titres were determined by
506 collecting groups of six *25174* and *25174*^{seml} flies infected in the same way as in survival experiments,
507 starting at 0h and then every 12h for 48h. Flies were anaesthetised with CO_2 before homogenisation in ice-
508 cold TSB. Homogenates were kept on ice and serially diluted in fresh ice cold TSB. 100µL of pre-determined
509 dilutions were plated by spreading on TSA to achieve colony counts of ~30-300 colonies. Platings were
510 made in duplicate. Plates were incubated for 24-30h at 30°C and photographed. Bacterial colonies were
511 enumerated using OpenCFU [55]. Data were collected in two blocks for *25174* flies. It was verified that
512 NCTC counts were similar between blocks (**S3 Fig**, see also **Fig. 5b**) and data were combined for analysis.
513
514 To assess the immunostimulatory capacity of spent culture supernatants *D. melanogaster DD1* and *DD1*^{seml}
515 flies were injected with spent culture supernatant and groups of 6 flies were collected 18h after injection for
516 imaging and assessment of GFP production. Live *D. melanogaster* flies were anaesthetised on a CO_2 pad
517 and imaged using an Olympus SZX-TLGAD microscope with a MVPLAPO 1X lens. Samples were
518 illuminated using a Cool LED pE-2 colluminator and photographed using a RETIGA R3 MONO camera. GFP
519 signal was quantified by selecting the areas of the images occupied by flies and taking measurements of the
520 measured area (A), the integrated density (ID) of the area (the product of the area measured and the mean
521 grey value of that area), and mean grey value of the background (GB) before calculating CTF as follows;
522
523 $$CTF = ID - (A \times GB)$$
524
525 These values were then averaged over the number of flies imaged, and normalised to CTF values extracted
526 from TSB-injected flies. Presentation images were prepared using Fiji [57]. Contrast of entire images was
527 adjusted for presentation purposes, ensuring no clipping of high or low signals.
528
529 **Lysozyme resistance assays**
530 Lysozyme resistance assays were carried out as in [30]. *S. aureus* cells from an overnight culture were
531 collected by centrifugation, washed once with PBS (10mM Na_2PO_4, 150mM NaCl, pH 6.5), and adjusted to
532 an OD_{600} of 0.4 in 50 ml of PBS. 20mL of suspension was placed into two 100mL flasks and incubated with or
533 without 300 µg mL^{-1} lysozyme (final concentration; Sigma) for 6h with shaking at 30°C. Bacterial lysis was
534 monitored by following OD_{600} and the percentage of bacterial lysis was calculated as the OD_{600} at a given
535 time point divided by OD_{600} at 0h, multiplied by 100.

536

537 **Peptidoglycan isolation and analysis by reverse-phase high-performance liquid chromatography**

538 PGN was prepared from exponential phase (OD_{600} 0.5-0.9) and stationary phase cells (24h post-inoculation)
539 as previously described [33]. Briefly, cells were chilled in an ice-ethanol bath and harvested by centrifugation,
540 resuspended in 20mL Milli-Q water and then transferred to 40mL boiling 8% (w/v) sodium dodecyl sulphate
541 (SDS) with stirring. Samples were boiled for 30 minutes, cooled to RT and stored overnight at 4°C. Samples
542 were re-boiled, and SDS washed out with repeated washing with warm MilliQ water and centrifugation. SDS-
543 free pellets were stored at -80°C.

544

545 Defrosted pellets were then homogenised with fine acid-washed glass beads in a FastPrep-24 Classic.
546 Unbroken debris was pelleted, supernatants were retained and treated first with DNAse I and RNAse I
547 (Sigma), then with Trypsin (Sigma). SDS was again added to a concentration of 1% (w/v) and samples
548 boiled. Samples were washed with Milli-Q water, then resuspended in 8M LiCl for 15min at 37°C. Samples
549 were pelleted, resuspended in EDTA (100mM, pH 7.0) and incubated for a further 15min at 37°C, washed
550 once more with Milli-Q water, resuspended in acetone and sonicated for 5min. Samples were washed twice
551 more and resuspended in MilliQ water before overnight lyophilisation at 30°C. Samples were resuspended in
552 MilliQ water to a final concentration of 20mg mL^{-1}.

553

554 To remove teichoic acids, samples were treated with hydrofluoric acid (46% v/v) and incubated at 4°C for
555 48h. Samples were iteratively washed with Tris-HCl until the pH of the supernatant reached pH 7.0-7.5.
556 Samples were then washed with MilliQ water twice. Samples were finally resuspended in MiliQ water,
557 lyophilised overnight and resuspended to a final concentration of 20mg mL^{-1}.

558

559 Muropeptides were prepared by digestion with mutanolysin (Sigma), reduced with sodium borohydride
560 (Sigma) and analyzed by reverse-phase HPLC using a Hypersil ODS C-18 column (Thermo Electron
561 Corporation) using a Shimadzu Prominence HPLC system using a 5-30% v/v methanol gradient in $NaHPO_4$
562 at pH2.0. Sample absorbance was measured at 206nm. Data analysis was performed using Shimadzu
563 prominence software and peaks identified where possible from comparison to previous work [58,59] and
564 reference HPLC profiles from the Bacterial Cell Surfaces and Pathogenesis Lab (S. Filipe, ITQB, Oeiras,
565 Portugal).

566

567 **Electron Microscopy**

568 Bacteria from overnight cultures were inoculated into fresh TSB at an initial OD_{600} of 0.05 and grown for 24h.
569 Cells were then collected by centrifugation, resuspended in 1mL 1% glutaraldehyde (w/v) and 1% osmium
570 tetroxide (w/v) in 0.1M PIPES buffer on ice (0.058g L^{-1} NaCl, 0.3g L^{-1} piperazine-N,N'bis[2-ethanesulfonic
571 acid], 0.02g L^{-1} $MgCl_2 \cdot 6H_2O$, 0.1M NaOH) and incubated at 4°C for 1h. Samples were washed with PIPES
572 buffer and then 4 times with MilliQ water, left for 5-10 minutes between each MilliQ wash. Samples were
573 embedded in 4% (w/v) low melting point agarose in 0.1M PIPES buffer, cut into ~1mm^3 pieces, and
574 incubated in 0.5% uranyl acetate overnight at 4°C in the dark. Samples were then rinsed with MilliQ water for
575 10min.
576
577 Samples were then serially incubated on ice in ice-cold 30%, 50%, 70%, 80%, 90% (all v/v) ethanol followed
578 by two incubations in 100% ethanol, for 10min each. Samples were placed in anhydrous ice-cold acetone at
579 RT for 10min. Samples were transferred to RT anhydrous acetone for another 20min. Samples were then
580 infiltrated with low viscosity resin (TLVR; TAAB Laboratory and Microscopy equipment) by incubation in 3:1
581 acetone:TLVR for 1h and then 1:1 acetone:TLVR for for 2h and finally 1:3 acetone:TLVR, with rotation.
582 Samples were incubated in TLVR overnight at RT. Resin was changed the next morning and again after
583 another 4h.
584
585 Samples were embedded in Beem capsules filled with TLVR and resin polymerised at 60°C for 24h. Sample
586 blocks were removed using a razor blade and ultra-thin sections made using a Diatome diamond knife using
587 a Leica UC7 ultramicrotome and mounted on 200 mesh Cu grids. Grids were placed section-side down on a
588 droplet of Reynolds lead-citrate and incubated at RT for 5min. Grids were washed by passing over a droplet
589 of degassed MilliQ water, 5 times. Grids were then blotted dry and left to dry completely. Imaging was
590 performed at 120kV using an FEI Technai 12 transmission electron microscope. Images were acquired using
591 a Gatan OneView CMOS camera with Digital Micrograph 3.0 software.
592
593 **Statistical analyses**
594 All statistical analyses were performed using R [60]. Statistical models were built including all possible
595 interactions first (maximal models) and where appropriate (i.e. if interaction terms had little or no explanatory
596 power) iterative model simplification was performed via likelihood ratio testing [61] with highest order non-
597 significant interactions removed first. Non-significant interaction effects were incrementally removed and the
598 fit of the original model and simplified model compared by ANOVA until the minimum adequate model was
599 obtained. These models were used for analyses. General linear models were employed where possible, but

where data exhibited violations of the assumptions of general linear modelling, data were transformed to conform to assumptions or generalised linear models were used instead, as most appropriate. Normality was assessed using the Shapiro-Wilk test. Error structures and link functions were chosen for generalised linear models following interpretation of diagnostics of their cognate general linear models and iterative improvement of model fitting to the data. Results are given from ANOVA tables where general linear models were used and ANODE tables for generalised linear models. ANOVA table results are presented as the F-statistic with degrees of freedom (df) in subscript and the model term in superscript, followed by the *p*-value ($\text{F-statistic}_{df}^{model_term}$ = N, p-value = n) . ANODE table results are presented as the Chi-squared (χ^2) statistic, followed by the df and the p-value ($\text{Chi-sq}^{model_term}$ = N, df = x, p = n). Contrasts made were THSD post-hoc contrasts.

Author contributions

Design of experiments: **JD, MLA, JM, PL, SRF**

Experimental work: **JD, MLA, EP, EJ, AP**

Analysis of data: **JD, EP**

Writing of the paper: **JD, SRF, PL**

Acknowledgements

JD was supported by a Wellcome Trust Infection, Immunity and Translational Medicine Scholarship. We acknowledge the Sir William Dunn School of Pathology Electron Microscopy Facility for support with sample preparation and imaging.

Figure Captions

Figure 1. Schematic representation of peptidoglycan recycling in *S. aureus* and genomic organisation of peptidoglycan recycling genes. **a** PGN is cleaved by Atl, a bifunctional enzyme with *N*-acetylmuramoyl-L-alanine amidase (blue arrows) and *N*-acetylglucosaminidase (red arrows) activity, along with other PGN hydrolases, to produce MurNAc-GlcNAc fragments (see **Introduction**). These fragments are taken-up and phosphorylated via MurP and metabolised cytoplasmically by MupG, MurQ and NagA. The PR components studied here are shown in colour. The 'periplasm' is labelled following Matias *et al.* [62]. **b** The genes encoding PR genes *mupG, murQ* and *murP* are encoded in an operon along with *murR* (orange line), whereas *nagA* is not part of an operon.

631

632 **Figure 2.** Growth of peptidoglycan recycling mutants. PR mutants were inoculated into fresh tryptic soy broth
633 (TSB) at an initial OD_{600} of 0.05 and grown for a period of 72h. The mean OD_{600} is shown by the dotted line,
634 and standard deviation (SD) of measurements by the shaded areas. Data are from 3 independent biological
635 replicates. Further quantification of key growth parameters can be found in **S2 Table**.

636

637 **Figure 3.** GlcNAc-6-P accumulation in Δ*nagA* throughout growth. Cytoplasmic content of bacteria grown in
638 TSB was extracted and subjected to IC-MS/MS to quantify intracellular metabolites. GlcNAc-6-P abundance
639 was extracted from the dataset through comparison to a reference peak generated by examination of the
640 purified compound (see **Materials and Methods**). Data were normalised to the total abundance of all
641 detected metabolites. cps; counts per second. Median abundance is indicated by the thick black line, while
642 the upper and lower quartiles are given by the upper and lower limits of boxes. The upper and lower limits of
643 the data are denoted by box whiskers. Letters given above boxes represent THSD contrasts across time
644 points, within each strain. Samples bearing the same letter were not statistically different. Asterisks denote
645 Tukey's honest significant differences (THSD) post-hoc contrasts between strains; *** $p < 0.001$. Data are
646 from 5 independent biological replicates.

647

648 **Figure 4.** Viability of peptidoglycan recycling mutants under nutrient limitation. The number CFU present in
649 cultures of each PR mutant at the given time points throughout growth in TSB was enumerated by plating on
650 tryptic soy agar (TSA). The median CFU is indicated by the thick black line, while the upper and lower
651 quartiles are given by the upper and lower limits of boxes. The upper and lower limits of the data are denoted
652 by box whiskers. Letters given above boxes represent THSD contrasts across strains, within each time point.
653 Samples bearing the same letter were not statistically different. Data are from 3 independent biological
654 replicates.

655

656 **Figure 5.** Infection of *D. melanogaster* by peptidoglycan recycling mutants. **a** *D. melanogaster 25174* flies
657 were injected with 100-200 CFU of each of the PR mutants and *Δatl.* Their survival was monitored at 12h
658 intervals over the course of 72h and estimated survival curves were constructed from the data. Lines
659 represent mean estimated survival and shaded regions represent the 95% confidence intervals. Asterisks
660 denote THSD post-hoc contrasts between strains; * $p < 0.05$, ** $p < 0.01$, *** $p < 0.001$. Data are from 9
661 independent biological replicates. Sample sizes, in number of flies injected; NCTC = 580, Δ*murP* = 312,
662 Δ*murQ* = 299, Δ*nagA* = 306, Δ*atl* = 289, PBS = 289. **b** *D. melanogaster 25174* flies were again injected with

663 100-200 CFU of each of the PR mutants and *Δatl*, but this time the bacterial load (number of viable CFU fly^{-1})
664 was enumerated every 12h for 48h. Data were box-cox transformed for analysis. AU; arbitrary units. A
665 comparison between the original untransformed data and box-cox transformed data can be found in **S3**
666 **Table**. The median box-cox transformed bacterial load is given by the thick black line, while the upper and
667 lower quartiles are given by the upper and lower limits of boxes. The upper and lower limits of the data are
668 denoted by box whiskers. Letters given above boxes represent THSD contrasts across strains, within each
669 time point. Samples bearing the same letter were not statistically different. Data are from 3 independent
670 biological replicates, performed in 2 blocks (6 replicates for NCTC). No difference in the bacterial load was
671 detected in NCTC between the two replicates (**S3 Fig**; ANOVA; $F_{1, 24}^{experimental_block} = 1.24$, $p = 0.28$).
672
673 **Figure 6.** Stimulation of *D. melanogaster* immune response by spent peptidoglycan recycling mutant culture
674 supernatant. SCS from overnight cultures of PR mutants were injected into either *DD1* (functional PGRP-SA)
675 or *DD1*^{seml} (non-functional PGRP-SA) flies. 18h later, flies were imaged to quantify Drosomycin::GFP
676 fluorescence as a proxy for Toll-cascade activation and normalised corrected total fluorescence calculated
677 from obtained images (see **Materials and Methods**). AU; arbitrary units. The median fluorescence is given
678 by the thick black line, while the upper and lower quartiles are given by the upper and lower limits of boxes.
679 The upper and lower limits of the data are denoted by box whiskers. Letters given above boxes represent
680 THSD contrasts across fly lines, within each bacterial strain. Samples bearing the same letter were not
681 statistically different. Asterisks denote THSD post-hoc contrasts between bacterial strains in *DD1* flies; * $p <$
682 0.05, *** $p < 0.001$. Data are from 3 independent biological replicates. Representative images of flies injected
683 with SCS from each bacterial strain are shown below the plot.
684
685 **Figure 7.** Infection of PGRP-SA deficient *D. melanogaster* by peptidoglycan recycling mutants. **a** *D.*
686 *melanogaster 25174*^{seml} flies were injected with 100-200 CFU of each of the PR mutants and *Δatl.* Their
687 survival was monitored at 12h intervals over the course of 72h and estimated survival curves were
688 constructed from the data. Lines represent mean estimated survival and shaded regions represent the 95%
689 confidence intervals. Asterisks denote THSD post-hoc contrasts between strains; * $p < 0.05$, ** $p< 0.01$, *** p
690 < 0.001. Data are from 7 independent biological replicates, including 3 used for determination of *in vivo*
691 bacterial titres (**b**; see **Materials and Methods**). Sample sizes, in number of flies injected; NCTC = 236,
692 Δ*murP* = 196, Δ*murQ* = 192, Δ*nagA* = 195, Δ*atl* = 198, PBS = 127. **b** *D. melanogaster 25174*^{seml} flies were
693 again injected with 100-200 CFU of each of the PR mutants and *Δatl*, but this time the bacterial load was
694 measured every 12h for 48h. Data were box-cox transformed for analysis. AU; arbitrary units. A comparison

695 between the original untransformed data and box-cox transformed data can be found in **S3 Table**. The
696 median box-cox transformed bacterial load is given by the thick black line, while the upper and lower
697 quartiles are given by the upper and lower limits of boxes. The upper and lower limits of the data are denoted
698 by box whiskers. Letters given above boxes represent THSD contrasts across strains, within each time point.
699 Samples bearing the same letter were not statistically different. Data are from 3 independent biological
700 replicates.

701

702 **Figure 8.** Lysozyme susceptibility of peptidoglycan recycling mutants. Overnight cultures of PR mutants and
703 Δ*tagO* (see **S1 Table**) were washed and resuspended in PBS containing 300μg mL^{-1} lysozyme (+ lysozyme),
704 or no lysozyme (- lysozyme). OD_{600} was then monitored over 6h. % original OD_{600} (see **Materials and**
705 **Methods**) was calculated as a percentage of the OD_{600} of each strain at the start of the experiment. Mean %
706 original OD_{600} is given by either dotted (+ lysozyme) or dashed (- lysozyme) lines and shaded areas denote
707 SD. Data are from 3 independent biological replicates.

708

709 ## References

710 [1] Vollmer W, Blanot D, de Pedro M a. Peptidoglycan structure and architecture. FEMS Microbiol Rev
711 2008;32:149–67. https://doi.org/10.1111/j.1574-6976.2007.00094.x.

712 [2] Typas A, Banzhaf M, Gross C a., Vollmer W. From the regulation of peptidoglycan synthesis to
713 bacterial growth and morphology. Nat Rev Microbiol 2012;10:123–36.
714 https://doi.org/10.1038/nrmicro2677.

715 [3] Vermassen A, Leroy S, Talon R, Provot C, Popowska M, Desvaux M. Cell wall hydrolases in bacteria:
716 Insight on the diversity of cell wall amidases, glycosidases and peptidases toward peptidoglycan.
717 Front Microbiol 2019;10. https://doi.org/10.3389/fmicb.2019.00331.

718 [4] Wong W, Young FE, Chatterjee AN. Regulation of Bacterial Cell Walls : Turnover of Cell Wall in
719 Staphylococcus aureus. J Bacteriol 1974;120:837–43.

720 [5] Blumel P, Uecker W, Giesbrecht P. Zero order kinetics of cell wall turnover. Arch Microbiol
721 1979;121:103–10.

722 [6] Goodell EW. Recycling of Murein by Escherichia coli. J Bacteriol 1985;163:305–10.

723 [7] Mauck J, Chan L, Glaser L. Turnover of the Cell Wall of Gram-positive Bacteria. J Biol Chem
724 1971;246:1820–7.

725 [8] Goodell EW, Schwarz U. Release of cell wall peptides into culture medium by exponentially growing
726 Escherichia coli. J Bacteriol 1985;162:391–7.

727 [9] Reith J, Mayer C. Peptidoglycan turnover and recycling in Gram-positive bacteria. Appl Microbiol
728 Biotechnol 2011;92:1–11. https://doi.org/10.1007/s00253-011-3486-x.

729 [10] Mayer C, Kluj RM, Mühleck M, Walter A, Unsleber S, Hottmann I, et al. Bacteria's different ways to
730 recycle their own cell wall. Int J Med Microbiol 2019;309:151326.
731 https://doi.org/10.1016/j.ijmm.2019.06.006.

[11] Borisova M, Gaupp R, Duckworth A, Schneider A, Dalügge D, Mühleck M, et al. Peptidoglycan recycling in gram-positive bacteria is crucial for survival in stationary phase. MBio 2016;7:1–10. https://doi.org/10.1128/mBio.00923-16.

[12] Kluj RM, Ebner P, Adamek M, Ziemert N, Mayer C, Borisova M. Recovery of the peptidoglycan turnover product released by the Autolysin Atl in staphylococcus aureus involves the phosphotransferase system transporter MurP and the Novel 6-phospho-N-acetylmuramidase MupG. Front Microbiol 2018;9. https://doi.org/10.3389/fmicb.2018.02725.

[13] Park JT, Uehara T. How bacteria consume their own exoskeletons (turnover and recycling of cell wall peptidoglycan). Microbiol Mol Biol Rev 2008;72:211–27. https://doi.org/10.1128/MMBR.00027-07.

[14] Jacobs C, Huang L, Bartowsky E, Normark S, Park JT. Bacterial cell wall recycling provides cytosolic muropeptides as effectors for beta-lactamase induction. EMBO J 1994;13:4684–94.

[15] Uehara T, Suefuji K, Valbuena N, Donegan M, Park JT. Recycling of the Anhydro-N-Acetylmuramic Acid Derived from Cell Wall Murein Involves a Two-Step Conversion to N-Acetylglucosamine-Phosphate. J Bacteriol 2005;187:3643–9. https://doi.org/10.1128/JB.187.11.3643.

[16] Jaeger T, Arsic M, Mayer C. Scission of the lactyl ether bond of N-acetylmuramic acid by Escherichia coli “etherase.” J Biol Chem 2005;280:30100–6. https://doi.org/10.1074/jbc.M502208200.

[17] Dahl U, Jaeger T, Nguyen BT, Sattler JM, Mayer C. Identification of a Phosphotransferase System of Escherichia coli Required for Growth on N-Acetylmuramic Acid. J Bacteriol 2004;186:2385–92. https://doi.org/10.1128/JB.186.8.2385-2392.2004.

[18] White B, Pasternak C. The Purification and Properties of N-Acetylglucosamine 6-Phosphate Deacetylase from *Escherichia coli*. Biochem J 1967;105:121–125. https://doi.org/10.1042/bj1050121.

[19] Komatsuzawa H, Fujiwara T, Nishi H, Yamada S, Ohara M, McCallum N, et al. The gate controlling cell wall synthesis in Staphylococcus aureus. Mol Microbiol 2004;53:1221–31. https://doi.org/10.1111/j.1365-2958.2004.04200.x.

[20] Bera A, Herbert S, Jakob A, Vollmer W, Götz F. Why are pathogenic staphylococci so lysozyme resistant? The peptidoglycan O-acetyltransferase OatA is the major determinant for lysozyme resistance of Staphylococcus aureus. Mol Microbiol 2005;55:778–87. https://doi.org/10.1111/j.1365-2958.2004.04446.x.

[21] Stapleton MR, Horsburgh MJ, Hayhurst EJ, Wright L, Jonsson I-M, Tarkowski A, et al. Characterization of IsaA and SceD, two putative lytic transglycosylases of Staphylococcus aureus. J Bacteriol 2007;189:7316–25. https://doi.org/10.1128/JB.00734-07.

[22] Zhu Y, Nandakumar R, Sadykov MR, Madayiputhiya N, Luong TT, Gaupp R, et al. RpiR homologues may link Staphylococcus aureus RNAIII synthesis and pentose phosphate pathway regulation. J Bacteriol 2011;193:6187–96. https://doi.org/10.1128/JB.05930-11.

[23] Amoroso A, Boudet J, Berzigotti S, Duval V, Teller N, Mengin-Lecreulx D, et al. A peptidoglycan fragment triggers beta-lactam resistance in Bacillus licheniformis. PLoS Pathog 2012;8:e1002571. https://doi.org/10.1371/journal.ppat.1002571.

[24] Moynihan PJ, Cadby IT, Veerapen N, Jankute M, Crosatti M, Mukamolova G V., et al. The hydrolase LpqI primes mycobacterial peptidoglycan recycling. Nat Commun 2019;10:1–11. https://doi.org/10.1038/s41467-019-10586-2.

[25] Jacobs C, Frère J-M, Normark S. Cytosolic intermediates for cell wall biosynthesis and degradation control inducible B-lactam resistance in Gram-negative bacteria. Cell 1997;88:823–32.

[26] Folkesson A, Eriksson S, Andersson M, Park JT, Normark S. Components of the peptidoglycan-recycling pathway modulate invasion and intracellular survival of Salmonella enterica serovar Typhimurium. Cell Microbiol 2005;7:147–55. https://doi.org/10.1111/j.1462-5822.2004.00443.x.

[27] Chan JM, Dillard JP. Neisseria gonnorhoeae crippled its peptidoglycan fragment permease to facilitate toxic peptidoglycan monomer release. J Bacteriol 2016:JB.00437-16. https://doi.org/10.1128/JB.00437-16.

[28] Nigro G, Fazio LL, Martino MC, Rossi G, Tattoli I, Liparoti V, et al. Muramylpeptide shedding modulates cell sensing of Shigella flexneri. Cell Microbiol 2008;10:682–95. https://doi.org/10.1111/j.1462-5822.2007.01075.x.

[29] Vitko NP, Grosser MR, Khatri D, Lance TR, Richardson AR. Expanded glucose import capability affords Staphylococcus aureus optimized glycolytic flux during infection. MBio 2016;7:1–11. https://doi.org/10.1128/mBio.00296-16.

[30] Reed P, Atilano ML, Alves R, Hoiczyk E, Sher X, Reichmann NT, et al. Staphylococcus aureus Survives with a Minimal Peptidoglycan Synthesis Machine but Sacrifices Virulence and Antibiotic Resistance. PLOS Pathog 2015;11:e1004891. https://doi.org/10.1371/journal.ppat.1004891.

[31] MacKay TFC, Richards S, Stone EA, Barbadilla A, Ayroles JF, Zhu D, et al. The Drosophila melanogaster Genetic Reference Panel. Nature 2012;482:173–8. https://doi.org/10.1038/nature10811.

[32] Atilano ML, Pereira PM, Vaz F, Catalão MJ, Reed P, Grilo IR, et al. Bacterial autolysins trim cell surface peptidoglycan to prevent detection by the Drosophila innate immune system. Elife 2014;3:1–23. https://doi.org/10.7554/eLife.02277.

[33] Filipe SR, Tomasz A, Ligoxygakis P. Requirements of peptidoglycan structure that allow detection by the Drosophila Toll pathway. EMBO Rep 2005;6:327–33. https://doi.org/10.1038/sj.embor.7400371.

[34] Pasztor L, Ziebandt A-K, Nega M, Schlag M, Haase S, Franz-Wachtel M, et al. Staphylococcal major autolysin (Atl) is involved in excretion of cytoplasmic proteins. J Biol Chem 2010;285:36794–803. https://doi.org/10.1074/jbc.M110.167312.

[35] Litzinger S, Duckworth A, Nitzsche K, Risinger C, Wittmann V, Mayer C. Muropeptide rescue in Bacillus subtilis involves sequential hydrolysis by beta-N-acetylglucosaminidase and N-acetylmuramyl-L-alanine amidase. J Bacteriol 2010;192:3132–43. https://doi.org/10.1128/JB.01256-09.

[36] Litzinger S, Fischer S, Polzer P, Diederichs K, Welte W, Mayer C. Structural and kinetic analysis of Bacillus subtilis N- acetylglucosaminidase reveals a unique Asp-His dyad mechanism. J Biol Chem 2010;285:35675–84. https://doi.org/10.1074/jbc.M110.131037.

[37] Reith J, Berking A, Mayer C. Characterization of an N-acetylmuramic acid/N-acetylglucosamine kinase of Clostridium acetobutylicum. J Bacteriol 2011;193:5386–92. https://doi.org/10.1128/JB.05514-11.

[38] Reith J, Mayer C. Characterization of a glucosamine/glucosaminide N-acetyltransferase of Clostridium acetobutylicum. J Bacteriol 2011;193:5393–9. https://doi.org/10.1128/JB.05519-11.

[39] Boersma MJ, Kuru E, Rittichier JT, Vannieuwenhze MS, Brun Y V, Winkler E. Minimal Peptidoglycan (PG) Turnover in Wild-Type and PG Hydrolase and Cell Division Mutants of Streptococcus pneumoniae D39 Growing Planktonically and in Host-Relevant Biofilms. J Bacteriol 2015;197:3472–85. https://doi.org/10.1128/JB.00541-15.Editor.

[40] Gaugué I, Oberto J, Putzer H, Plumbridge J. The Use of Amino Sugars by Bacillus subtilis: Presence of a Unique Operon for the Catabolism of Glucosamine. PLoS One 2013;8:1–12. https://doi.org/10.1371/journal.pone.0063025.

[41] Wheeler R, Turner RD, Bailey RG, Salamaga B, Mesnage S, Mohamad SAS, et al. Bacterial Cell Enlargement Requires Control of Cell Wall Stiffness Mediated by Peptidoglycan Hydrolases. MBio 2015;6:e00660-15. https://doi.org/10.1128/mBio.00660-15.Editor.

822 [42] Sugai M, Komatsuzawa H, Akiyama T, Hong YM, Oshida T, Miyake Y, et al. Identification of endo-
823 beta-N-acetylglucosaminidase and N-acetylmuramyl-L-alanine amidase as cluster-dispersing
824 enzymes in Staphylococcus aureus. J Bacteriol 1995;177:1491–6.

825 [43] Yamada S, Sugai M, Komatsuzawa H, Nakashima S, Oshida T, Matsumoto A, et al. An autolysin ring
826 associated with cell separation of Staphylococcus aureus. J Bacteriol 1996;178:1565–71.
827 https://doi.org/10.1128/jb.178.6.1565-1571.1996.

828 [44] Biswas R, Voggu L, Simon UK, Hentschel P, Thumm G, Götz F. Activity of the major staphylococcal
829 autolysin Atl. FEMS Microbiol Lett 2006;259:260–8. https://doi.org/10.1111/j.1574-6968.2006.00281.x.

830 [45] Doyle RJ, Chaloupka J, Vinter V. Turnover of cell walls in microorganisms. Microbiol Rev
831 1988;52:554–67.

832 [46] Mesnage S, Chau F, Dubost L, Arthur M. Role of N-acetylglucosaminidase and N-acetylmuramidase
833 activities in Enterococcus faecalis peptidoglycan metabolism. J Biol Chem 2008;283:19845–53.
834 https://doi.org/10.1074/jbc.M802323200.

835 [47] Boudreau M a, Fisher JF, Mobashery S. Messenger functions of the bacterial cell wall-derived
836 muropeptides. Biochemistry 2012;51:2974–90. https://doi.org/10.1021/bi300174x.

837 [48] Jaeger T, Mayer C. The transcriptional factors MurR and catabolite activator protein regulate N-
838 acetylmuramic acid catabolism in Escherichia coli. J Bacteriol 2008;190:6598–608.
839 https://doi.org/10.1128/JB.00642-08.

840 [49] Rudra P, Boyd JM. Metabolic control of virulence factor production in Staphylococcus aureus. Curr
841 Opin Microbiol 2020;55:81–7. https://doi.org/10.1016/j.mib.2020.03.004.

842 [50] Paracuellos P, Ballandras A, Robert X, Kahn R, Hervé M, Mengin-Lecreulx D, et al. The extended
843 conformation of the 2.9-Å crystal structure of the three-PASTA domain of a Ser/Thr kinase from the
844 human pathogen Staphylococcus aureus. J Mol Biol 2010;404:847–58.
845 https://doi.org/10.1016/j.jmb.2010.10.012.

846 [51] Ohlsen K, Donat S. The impact of serine/threonine phosphorylation in Staphylococcus aureus. Int J
847 Med Microbiol 2010;300:137–41. https://doi.org/10.1016/j.ijmm.2009.08.016.

848 [52] Arnaud M, Chastanet A, De M. New Vector for Efficient Allelic Replacement in Naturally Gram-
849 Positive Bacteria New Vector for Efficient Allelic Replacement in Naturally Gram-Positive Bacteria.
850 Appl Enviromental Microbiol 2004;70:6887–91. https://doi.org/10.1128/AEM.70.11.6887.

851 [53] Oshida T, Tomasz A. Isolation and Characterization of a Tn551-Autolysis Mutant of Staphylococcus
852 aureus. J Bacteriol 1992;174:4952–9.

853 [54] Kahm M, Hasenbrink G, Hella L-F, Ludwig J, Kschischo M. grofit : Fitting Biological Growth Curves
854 with R 2009:1–23.

855 [55] Geissmann Q. OpenCFU, a new free and open-source software to count cell colonies and other
856 circular objects. PLoS One 2013;8:e54072. https://doi.org/10.1371/journal.pone.0054072.

857 [56] Walsby-Tickle J, Gannon J, Hvinden I, Bardella C, Abboud MI, Nazeer A, et al. Anion-exchange
858 chromatography mass spectrometry provides extensive coverage of primary metabolic pathways
859 revealing altered metabolism in IDH1 mutant cells. Commun Biol 2020;3:1–12.
860 https://doi.org/10.1038/s42003-020-0957-6.

861 [57] Schindelin J, Arganda-Carreras I, Frise E, Kaynig V, Longair M, Pietzsch T, et al. Fiji: An open-source
862 platform for biological-image analysis. Nat Methods 2012;9:676–82.
863 https://doi.org/10.1038/nmeth.2019.

[58] De Jonge BLM, Chang YS, Gage D, Tomasz A. Peptidoglycan composition of a highly methicillin-resistant Staphylococcus aureus strain: The role of penicillin binding protein 2A. J Biol Chem 1992;267:11248–54.

[59] De Jonge BLM, Chang YS, Gage D, Tomasz A. Peptidoglycan composition in heterogeneous Tn551 mutants of a methicillin-resistant Staphylococcus aureus strain. J Biol Chem 1992;267:11255–9. https://doi.org/10.1111/emre.12151.

[60] R Core Team. R: A Language and Environment for Statistical Computing. R Found Stat Comput 2020;1:409. https://doi.org/10.1007/978-3-540-74686-7.

[61] Crawley MJ. The R Book. 2nd Edition. Danvers, MA, USA: Wiley-Blackwell; 2012.

[62] Matias VRF, Beveridge TJ. Native Cell Wall Organization Shown by Cryo-Electron Microscopy Confirms the Existence of a Periplasmic Space in Staphylococcus aureus. J Bacteriol 2006;188:1011–21. https://doi.org/10.1128/JB.188.3.1011.

Supplementary Figure and Table captions

S1 Figure. Abundance of key metabolites linking peptidoglycan recycling to peptidoglycan biosynthesis and central carbon metabolism. **a** Schematic representation of the downstream metabolism of GlcNAc-6-P resulting from PR. NagB is a GlcN-6-P deaminase, converting GlcN-6-P to Fru-6-P. GlmS is an amidotransferase which converts Fru-6-P to GlcN-6-P. Cytoplasmic content of bacteria grown in TSB was extracted and subject to IC-MS/MS to quantify intracellular metabolites, from the same dataset used to create **Figure 3**. GlcN-6-P (**b**) and Fru-6-P (**c**) abundance was extracted from the dataset through comparison to a pre-existing compound library (see **Methods**). The corresponding symbol from **a** is given in the top-right hand corner of each plot. Data were normalised to the total abundance of all detected metabolites. cps; counts per second. The median abundance is given by the thick black line, while the upper and lower quartiles are given by the upper and lower limits of boxes. The upper and lower limits of the data are denoted by box whiskers. Letters given above box plots represent THSD contrasts across time points, within each strain. Samples bearing the same letter were not statistically different. The asterisks denote the THSD post-hoc comparison between the two strains at 12h post-inoculation; *** $p < 0.001$. Data are from 5 independent biological replicates.

S2 Figure. Peptidoglycan muropeptide composition and cell wall ultrastructure of peptidoglycan recycling mutants. **a** CW PGN was purified from PR mutants after either 6h (exponential phase) or 24h (stationary phase) growth. Muropeptides produced from digestion of PGN samples (see **Materials and Methods**) were then analysed by RP-HPLC and detection by UV absorption at 206nm (A_{206nm}). Roman numerals I to V above the absorbance profile of NCTC for exponential phase indicate muropeptide monomers to pentamers. Peaks that differ in Δ*murP* are labelled **i** and **ii**. Peaks that differed in Δ*murQ* are shown in inset boxes and labelled

899 **iii**. The species corresponding to peaks **i** and **ii** were identified from [58,59] and are shown as an inset. M;
900 MurNac, G; GlcNAc. Peak **iii** was not identifiable by this method. **b** Cells from overnight cultures (Stationary
901 phase) were fixed and images acquired by transmission electron microscopy (see **Materials and Methods**).
902 The top row shows large fields of cells, and the lower rows high-magnification images of individual cells.
903 Scale bars in the top row of images represent 2μm and in the lower rows 200nm.
904
905 **S3 Figure.** Comparison of bacterial load over 2 experimental blocks presented in **Figure 5b**. Bacterial load
906 (number of viable CFU) per fly was enumerated every 12h for 48h. Data were box-cox transformed for
907 analysis. AU; arbitrary units. A comparison between the original untransformed data and box-cox transformed
908 data can be found in **S4 Table**. The median box-cox transformed bacterial load is given by the thick black
909 line, while the upper and lower quartiles are given by the upper and lower limits of boxes. The upper and
910 lower limits of the data are denoted by box whiskers. Each block consisted of 3 independent biological
911 replicates.
912
913 **S4 Figure.** Polymerase Chain Reaction confirmation of peptidoglycan recycling mutant construction and
914 absence of pMAD deletion vector. DNA was extracted from NCTC (WT; 'wild-type') or each of the mutants
915 constructed in this study (**S1 Table**) and subject to PCR analysis using primers listed in **S4 Table**. **a** The
916 absence of each of the target genes was confirmed using 'intA' and 'intB' primers. **b** The absence of the
917 vector used for gene deletion was confirmed using primers 'pMAD_p1' and 'pMAD_p2'. PCR product from
918 PCR performed on the empty pMAD vector (pMAD) was run as a control. **c** Expected PCR product sizes for
919 NCTC (WT) and each deletion mutant (Deletion mutant confirmation), and for each deletion vector (pMAD
920 screening). Sizes of DNA fragments in the DNA ladder (Ladder) are given to the left of each image. Original
921 gels from which lanes were selected are provided in **S5 Figure**.
922
923 **S5 Figure.** Lanes selected from original gels to produce **S4 Figure**. Orange arrows indicate the lanes which
924 were used to produce **S4 Figure**.

Dorling *et al*.

Analysis of the influence of peptidoglycan turnover and recycling on host-pathogen interaction in the Gram-positive pathogen *Staphylococcus aureus* (Peptidoglycan recycling and Gram-positive bacteria-host interaction)

MAIN FIGURES

Figure 1. Schematic representation of peptidoglycan recycling in *S. aureus* and genomic organisation of peptidoglycan recycling genes.

Figure 2. Growth of peptidoglycan recycling mutants.

Figure 3. GlcNAc-6-P accumulation in Δ*nagA* throughout growth.

Figure 4. Viability of peptidoglycan recycling mutants under nutrient limitation.

Figure 5. Infection of *D. melanogaster* by peptidoglycan recycling mutants.

Figure 6. Stimulation of *D. melanogaster* immune response by spent peptidoglycan recycling mutant culture supernatant

Figure 7. Infection of PGRP-SA deficient *D. melanogaster* by peptidoglycan recycling mutants.

Figure 8. Lysozyme susceptibility of peptidoglycan recycling mutants.

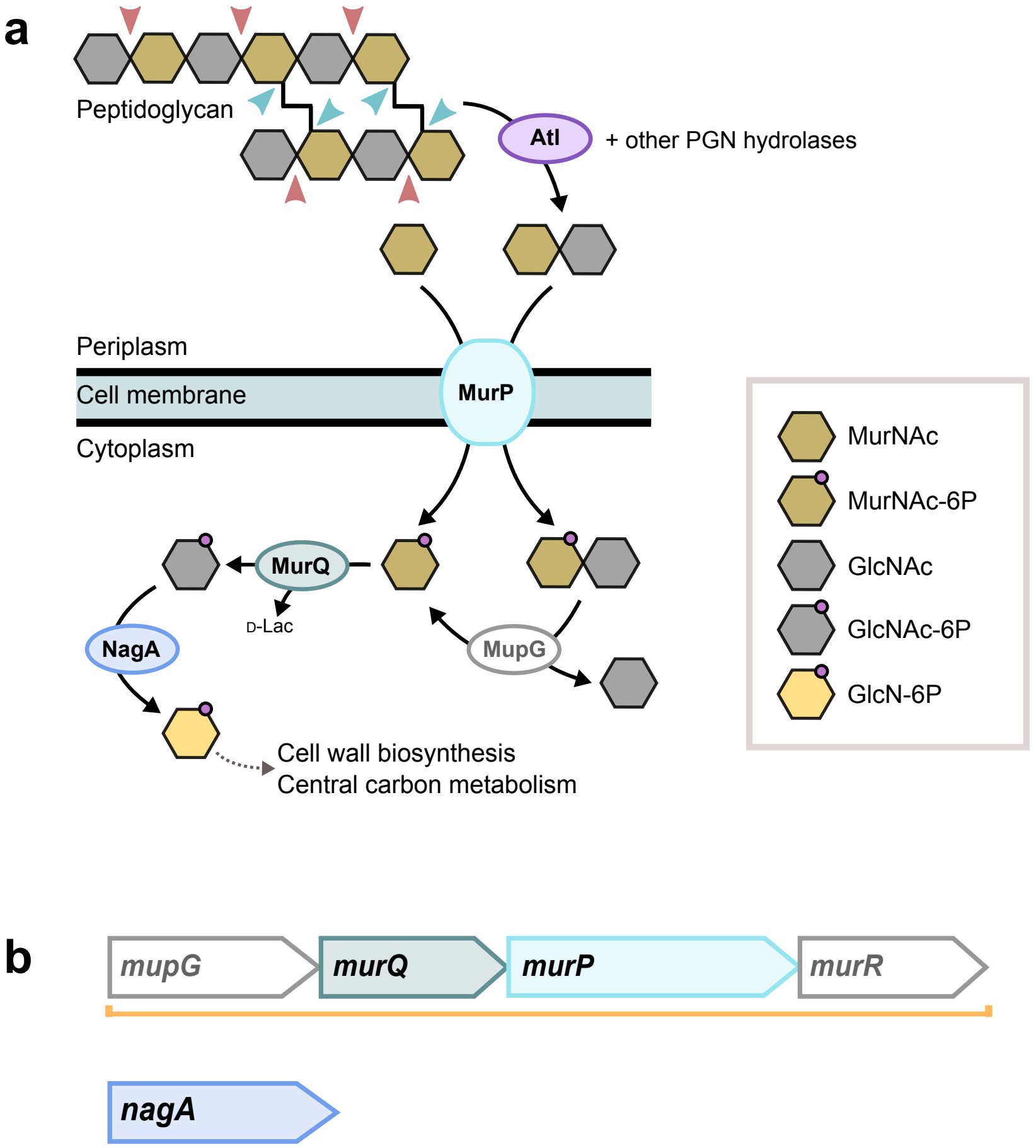
a
Peptidoglycan
Atl
+ other PGN hydrolases
Periplasm
Cell membrane
MurP
Cytoplasm
MurQ
D-Lac
NagA
MupG
Cell wall biosynthesis
Central carbon metabolism
MurNAc
MurNAc-6P
GlcNAc
GlcNAc-6P
GlcN-6P
b
mupG
murQ
murP
murR
nagA

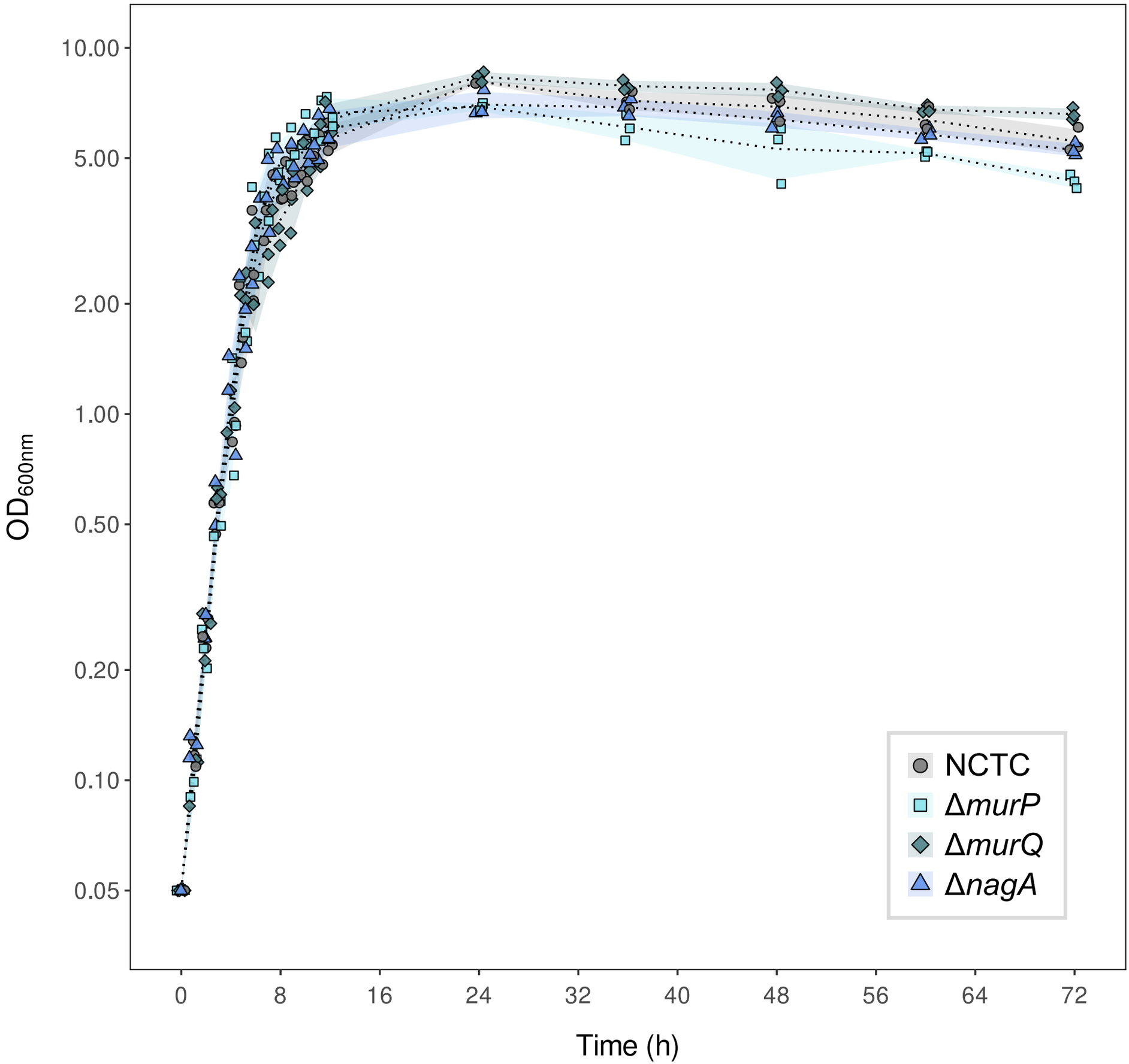
10.00
5.00
2.00
1.00
0.50
0.20
0.10
0.05
OD600nm
0
8
16
24
32
40
48
56
64
72
Time (h)
NCTC
ΔmurP
ΔmurQ
ΔnagA

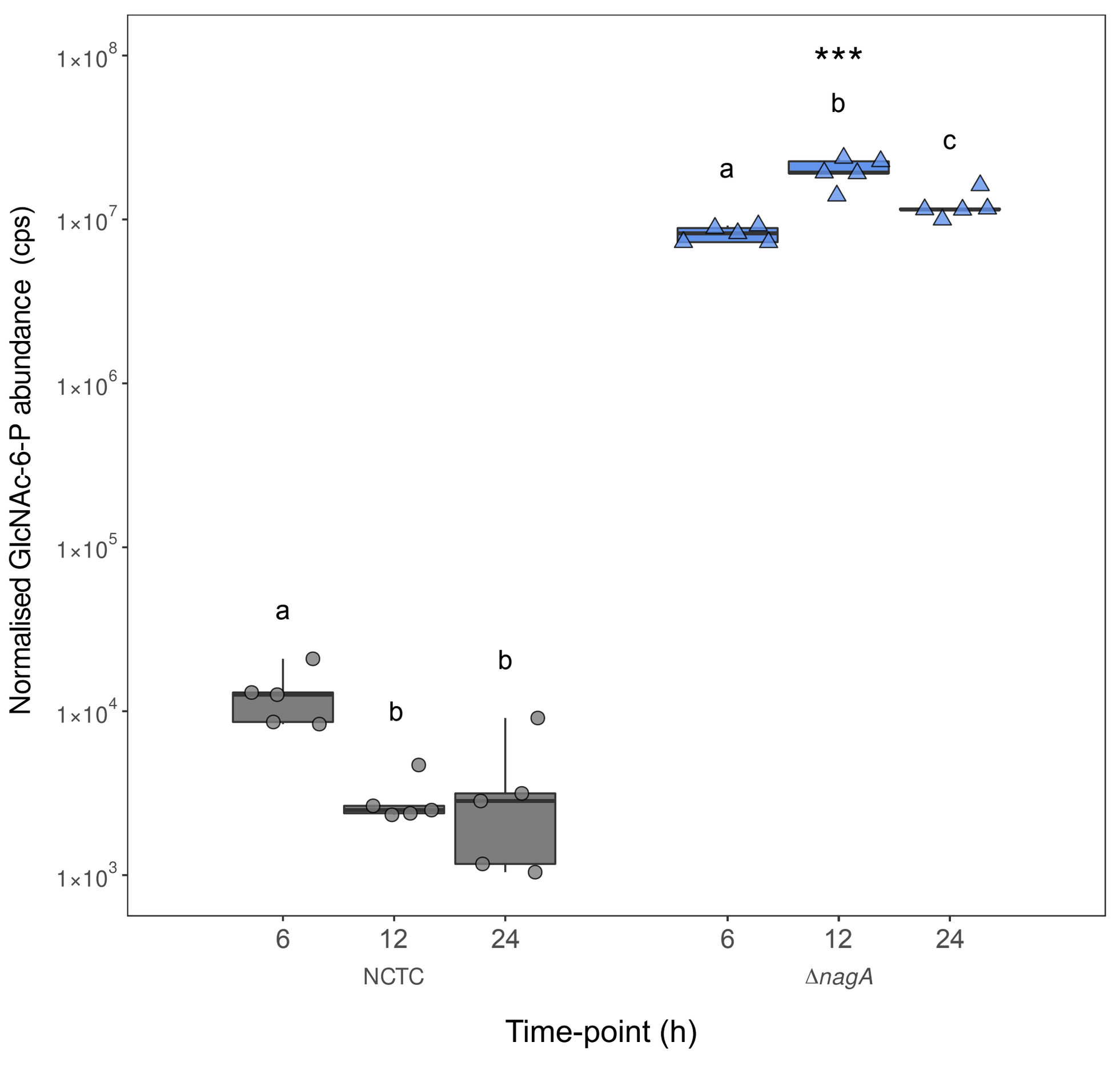
Normalised GlcNAc-6-P abundance (cps)
1×10^8
1×10^7
1×10^6
1×10^5
1×10^4
1×10^3
***
a
b
c
a
b
b
6
12
24
NCTC
6
12
24
ΔnagA
Time-point (h)

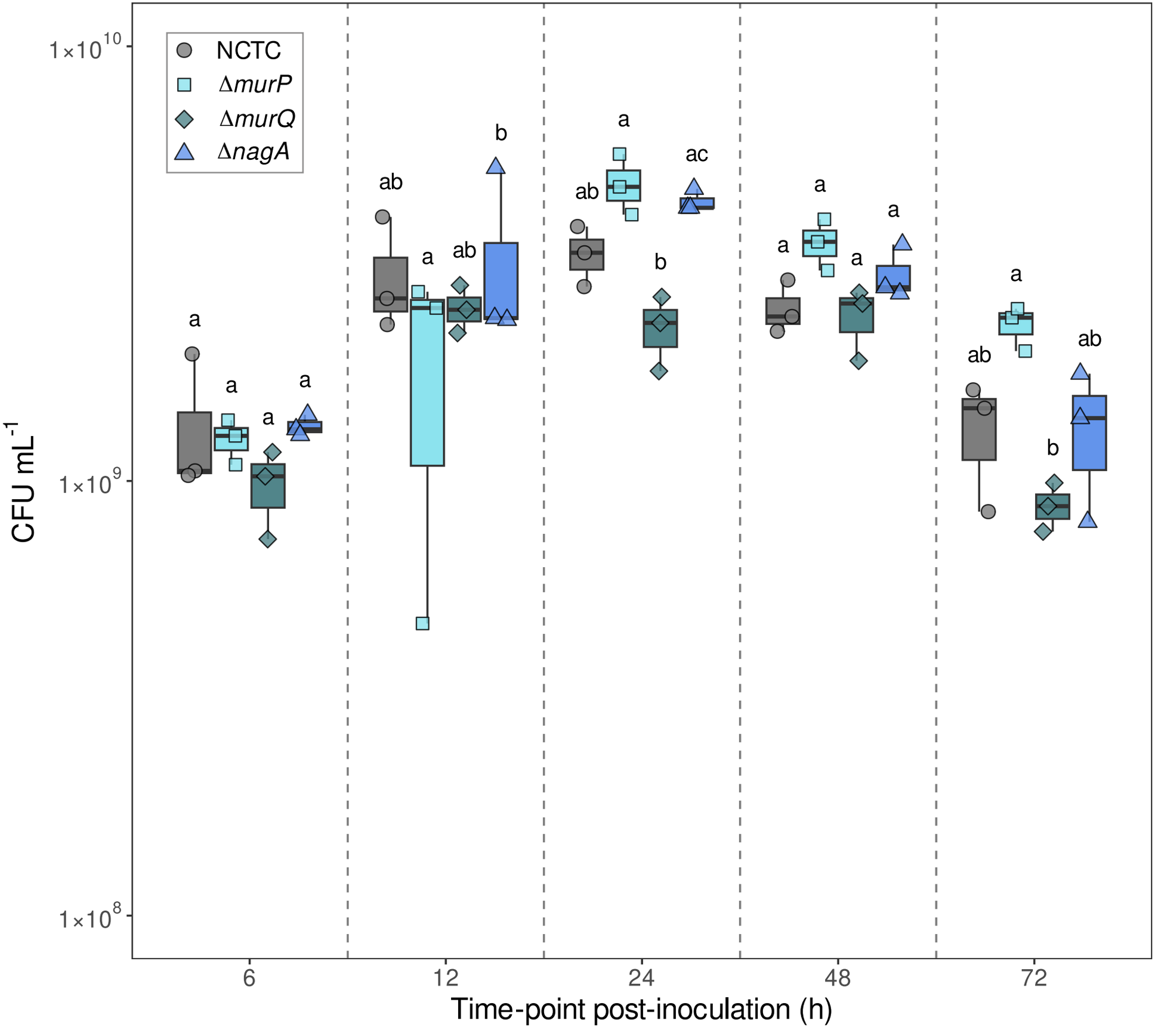
NCTC
ΔmurP
ΔmurQ
ΔnagA
1×10^10
1×10^9
1×10^8
CFU mL^-1
a
a
a
a
ab
a
ab
b
ab
a
ac
b
a
a
a
a
ab
a
ab
b
6
12
24
48
72
Time-point post-inoculation (h)

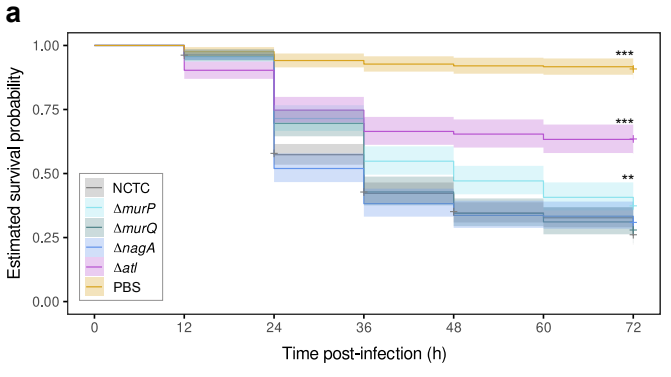
a
Estimated survival probability
1.00
0.75
0.50
0.25
0.00
0
12
24
36
48
60
72
Time post-infection (h)
NCTC
ΔmurP
ΔmurQ
ΔnagA
Δatl
PBS
***
***
**

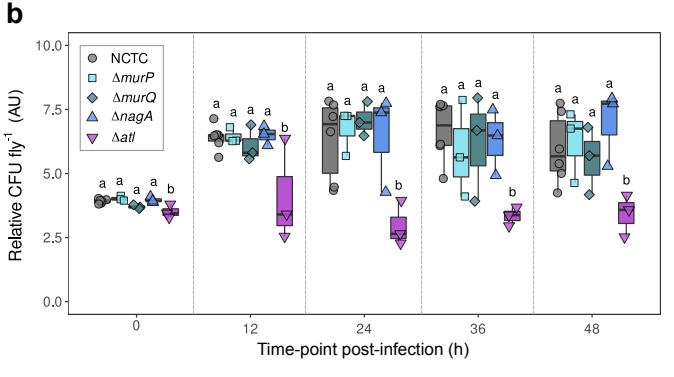
b
Relative CFU fly^{-1} (AU)
10.0
7.5
5.0
2.5
0.0
0
12
24
36
48
Time-point post-infection (h)
NCTC
ΔmurP
ΔmurQ
ΔnagA
Δatl

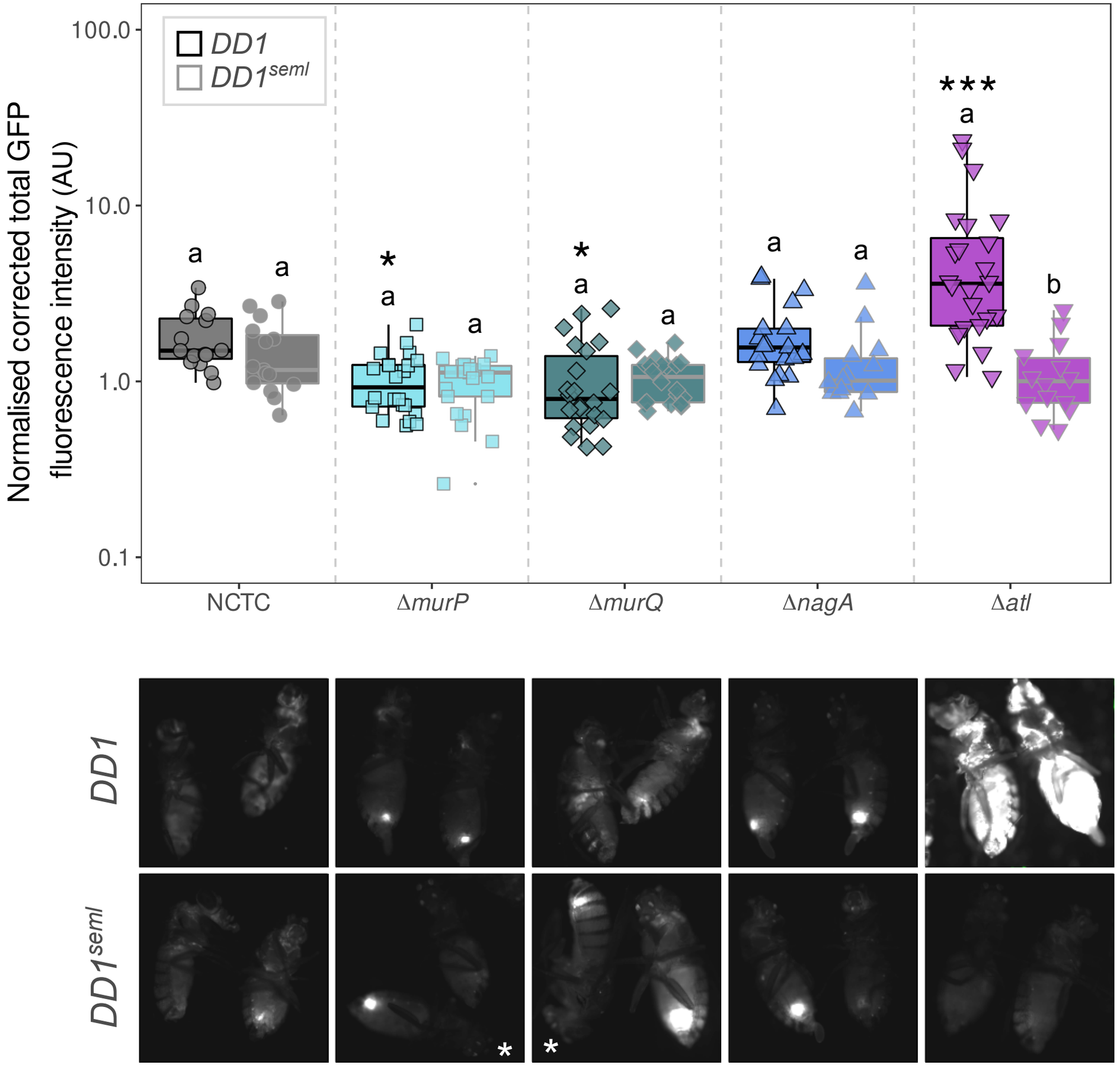
DD1
DD1seml
Normalised corrected total GFP fluorescence intensity (AU)
100.0
10.0
1.0
0.1
a
a
*
a
a
*
a
a
a
a
***
a
b
NCTC
ΔmurP
ΔmurQ
ΔnagA
Δatl
DD1
DD1seml
*
*

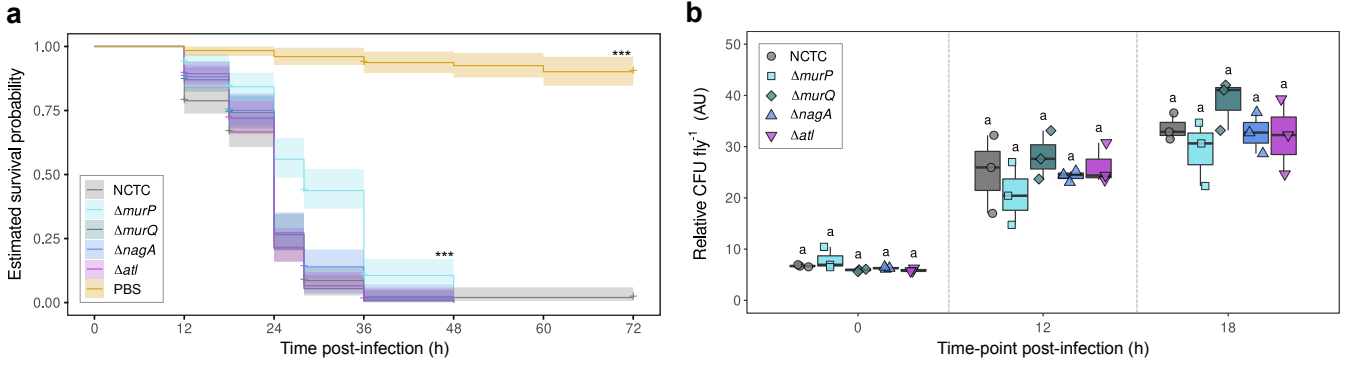
a
Estimated survival probability
1.00
0.75
0.50
0.25
0.00
0
12
24
36
48
60
72
Time post-infection (h)
NCTC
ΔmurP
ΔmurQ
ΔnagA
Δatl
PBS
***
***
b
Relative CFU fly-1 (AU)
50
40
30
20
10
0
0
12
18
Time-point post-infection (h)
NCTC
ΔmurP
ΔmurQ
ΔnagA
Δatl
a

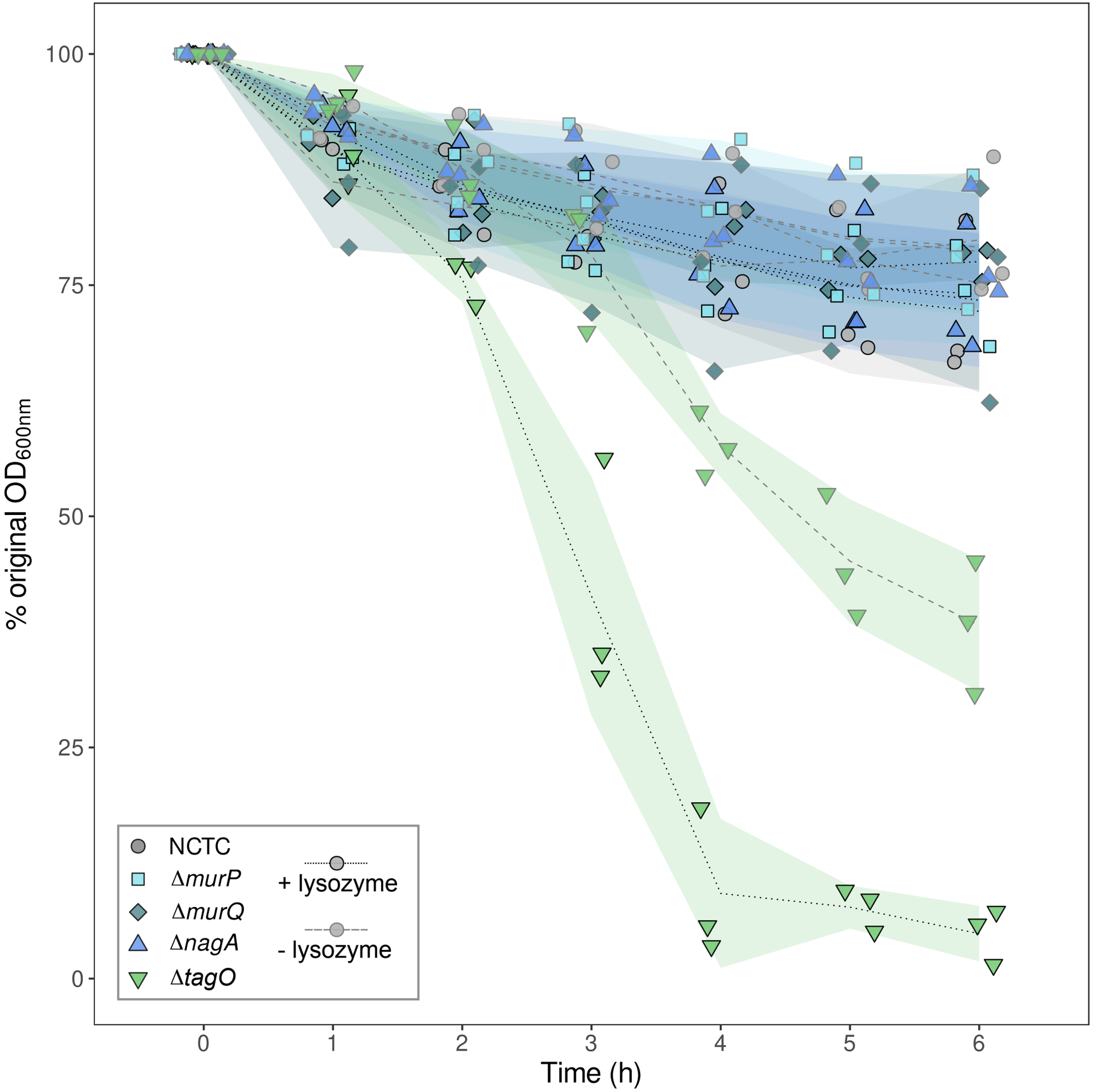
100
75
50
25
0
% original OD600nm
0
1
2
3
4
5
6
Time (h)
NCTC
ΔmurP
ΔmurQ
ΔnagA
ΔtagO
+ lysozyme
- lysozyme